UNITED NATIONS UNIVERSITY
GEOTHERMAL TRAINING PROGRAMME
Orkustofnun, Grensasvegur 9,
IS-108 Reykjavik, Iceland

Reports 2013
Number 5

1D INVERSION OF MT AND TEM DATA WITH APPLICATION OF SOUNDINGS FROM KRÝSUVÍK, SW-ICELAND AND A REVIEW OF MT/TEM DATA FROM BACMAN GEOTHERMAL PROJECT, CENTRAL PHILIPPINES

Jefferson R. Africa
Energy Development Corporation - EDC
38/F One Corporate Centre Building
Julia Vargas corner Meralco Avenue
Ortigas Center, Pasig City, 1605
PHILIPPINES
africa.jr@energy.com.ph

ABSTRACT

1D joint inversion and a study of selected MT and TEM soundings from the Krýsuvík high-temperature area, SW-Iceland and the Bacon-Manito geothermal project, Central Philippines was carried out using the TEMTD program. The two areas show a significant down shifting of MT apparent resistivity curves as a result of near-surface inhomogeneity. Joint inversion sections show a good correlation of the resistivity structure with the mineral alterations seen in the intersected wells although relic alteration was observed in both cases.

Inversion results highly depend on the initial model used and the parameters imposed. There exists a basement depth value where the fit of the inverted 1D model of the TEM and MT data varies significantly as depth becomes shallower or deeper than that value. The reliability of 1D joint inversion is highly dependent on the overlap of the TEM and MT data such that the downward bias of the MT apparent resistivity curve and the 3D structure effect of TEM data is reduced.

1. INTRODUCTION

Rapid industrialization demands an equally advancing technology. With this increasing technological capability, human beings can now automate a lot of things. But a huge amount of manageable energy is needed to keep up with the demands which human beings, we ourselves, have initially imposed. A lot of energy sources are now being utilized worldwide but only a small percentage is accounted for by renewable sources. Nonetheless, with the pressing issue of global warming, shifting towards renewable energy sources has been a long-term goal for humanity.

Among the renewable sources, geothermal energy has been utilized by people since time immemorial for direct utilization, but it plays a younger role in electricity generation. And, interestingly enough, only a small portion of the world‘s population is allocating work for geothermal energy development, which is to say that only 212 people per year per country (where countries considered are: 51% in Europe, 28% in Asia, 16% in America and 5% in Africa and Oceania) from the period of 2005-2009

expended time and effort on geothermal work (Lund et al., 2011). Nonetheless, geothermal development has progressed over the past few decades from a relatively small workforce.

In terms of geothermal developmental work, geo-scientific surface exploration has been mostly employed as a frontline procedure. The speculative work of exploration geoscientists like geophysicists resulted in a deep subsurface model, a reconstruction of data collected at the surface or near the surface of the ground. A lot of effort was made to improve the capability of scientists to "see through" the earth. There are a number of material properties like phase, density, conductivity, permeability and temperature and they play interdependently with one another. And the thin line that connects our devised models from the actual earth properties is our measuring and computing devices. The challenge for scientists is how to make sense out of the measured values and relate them to the intended subject, here a geothermal resource.

Cumulative work to improve scientific procedures and interpretation has culminated in today's capabilities. This report presents just a few of the geophysical tools which have contributed a lot in the geothermal industry. It presents some applications of electromagnetic methods and their processing schemes for geothermal prospecting.

2. PRINCIPLES

2.1 Resistivity of rocks

Electrical resistivity surveying is found to be the most useful tool in geothermal prospecting as it has a direct relationship with other material properties significant to a hydrothermal environment such as salinity, temperature and alteration (Hersir and Árnason, 2009). For the sake of simplicity, electrical resistivity/conductivity will be termed solely as resistivity/conductivity from now on and the terms will be used interchangeably. Most often, rocks behave as an Ohmic conductor/resistor having this simple relationship:

$$\rho = \frac{1}{\sigma} = \frac{|\vec{E}|}{|\vec{j}|} \tag{1}$$

where ρ = Resistivity (Ωm);
σ = Conductivity (S/m or 1/Ωm);
$|\vec{E}|$ = Electric field magnitude (V/m) (arrow on top signifies a vector quantity while vertical bars signify the magnitude component of the corresponding vector);
$|\vec{j}|$ = Current density (A/m^2).

Equation 1 states that under the constant influence of an electric field, the amount of charges passing through a section of rock at an interval of time decreases by the same factor that resistivity has increased or in the same way that its conductivity has decreased.

In a normal state, rocks behave as good resistors since electrons or ions within them are relatively bound. However, in a more natural setting, rocks interact with a lot of other substances like water and air and factors like temperature and pressure. Rock interactions with these other variables make their bulk resistivity highly variable.

Water plays a big role in altering the resistivity of rocks especially when it is saline and contains dissolved ions. Saline water is highly conductive compared to dry rock. As charges always flow through the region of least resistance, a rock in contact with saline water will, in effect, make the bulk resistivity lower since current will favour its flows with the ions dissolved in the water. In relation to this, the porosity of the rock matrix and its pore connectivity or effective porosity has a large effect on the

resistivity. Porosity itself can be defined as primary where interstices are originally present in the rock matrix and secondary where void spaces are created as a result of external factors such as pressure and erosion (Todd and Mays, 2005). At this point, it is noteworthy to include Archie's law (Archie, 1942) in the discussion which states that on a bi-logarithmic scale conductivity increases by a determined empirical factor with porosity.

$$\log \sigma = n \log \Phi_t + \log \sigma_w / a \quad (2)$$

where n = Cementing factor which is empirically determined; usually around 1-2;
Φ_t = Fractional porosity of the rock matrix;
σ_w = Conductivity of the fluid in the rock matrix (S/m);
a = Parameter depending on porosity type; empirically determined and usually around 1.

Temperature also plays a role in altering the bulk resistivity of the rock material and, again, an aqueous environment present in the rock matrix contributes much to this effect. The temperature is a measure of the average kinetic energy of a material such that, at higher temperatures, ionic movement is greatly enhanced, and thus conductivity in the same way. This relationship is more accurately defined by Dakhnov (1962):

$$\sigma_w = \sigma_{w0}[1 + \alpha(T - T_0)] \quad (3)$$

where σ_w = Conductivity of pore fluid (S/m) at temperature of T (°C);
σ_{w0} = Conductivity of pore fluid (S/m) at reference temperature of T_0 (°C);
T = Temperature at which σ_w is formed (°C);
α = Temperature coefficient of resistivity, i.e. $\alpha = 0.023$/°C for $T_0 = 25$°C

Equation 3 is valid only for a temperature range of 0-200°C and the behaviour starts to reverse as the temperature increases further. The Arrhenius formula shows this reverse change of a rock's electrical characteristics as the temperature approaches the melting point of the material. Thus, when approaching the heat source of a geothermal system where more than 400°C can be expected, one would observe an increase in the conductivity of the rock (Flóvenz et al., 2012).

In any case, the factors that can significantly alter the bulk resistivity of a rock in any hydrothermal environment are effective porosity of the rock matrix, salinity of the pore fluid and temperature.

In the instance that hot groundwater comes into contact with rock, the surface that is in direct contact with the hot fluid experiences secondary mineralization. This happens in such a way that as fluid flows through pores, some of their components are left in the rock or vice versa, restructuring them in the process. This is often referred to as hydrothermal alteration. It has a relevant effect on the conductivity of the rock being altered. Interestingly enough, alteration minerals vary depending on the temperature of the water coming into contact with it. Figure 1 shows the range of temperature values at which different alteration materials can be formed.

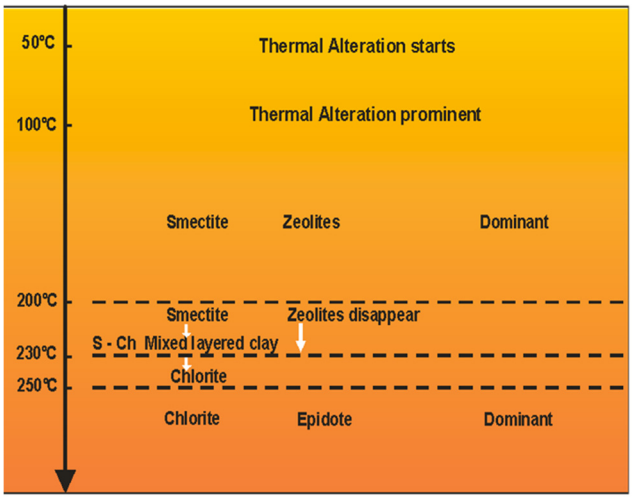

FIGURE 1: Formation temperature of different alteration minerals (adapted from Hersir and Árnason, 2009)

It has been found out that these alteration minerals contribute to a lot of differences in the bulk resistivity of the rock matrix as they themselves have different resistivity values. In a general sense, rock resistivity is affected by three main conduction mechanisms. The first

one is mineral conduction and has the least effect of conducting electrical current in a rock. This is contributed by the dry solid rock matrix itself. The next mechanism is pore fluid conduction; this is caused by moving ions within the heated saline groundwater. The last is surface conduction which is contributed mostly by the alteration minerals attached to the pore surface of the rock matter.

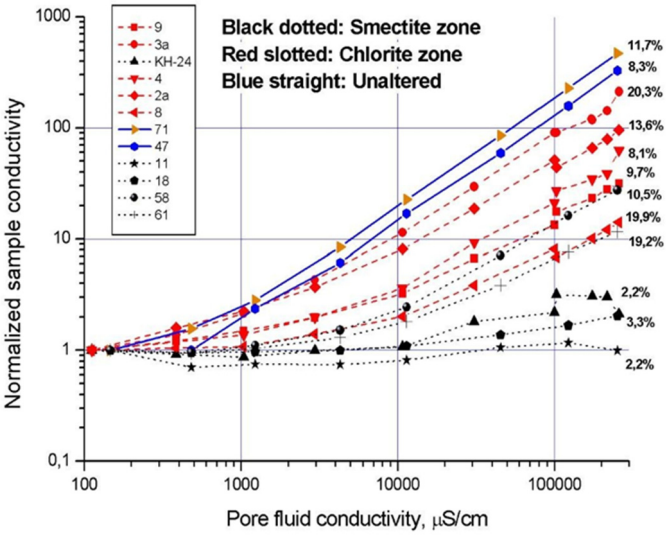

FIGURE 2: Bulk resistivity versus fluid conductivity at varying porosities (Flóvenz et al., 2005)

In a high-temperature geothermal environment, it is the alternating role of the last two conducting mechanisms that gives the contrast of resistivity at depth. The so-called "high-low-high" resistivity signature in this environment is caused by the presence of different alteration minerals which are formed and attached to the host rock at different temperatures. The low-temperature forming alterations like smectite and zeolite contain loosely bound ions contributing more to the surface conduction, hence to the bulk conductivity of the rock, than fluid conduction, while the high-temperature forming alterations like chlorite and epidote which have more bound ions contribute less to the conduction mechanism than pore fluid conduction itself. This behaviour is clearly illustrated in Figure 2. As the conductivity of the pore fluid in a rock is increased, its bulk conductivity is likewise increased. But the rate of increase is dictated by the type of minerals attached to the rock, whereby conductivity of the unaltered rock unit has higher sensitivity with the conductivity of the fluid than rocks with chlorite and smectite attached to them. The bulk conductivity of rock with smectite is least responsive to the change in the conductivity of the contained fluid.

The resistivity signature of rocks in a high-temperature geothermal environment may show three types of circumstances with reference to their temperature conditions. The existing temperature of the rocks can be in exact accordance with the formation temperatures of their secondary minerals and the measured resistivity. This means that the resistivity information can practically tell the present temperature distribution in the rocks. However, this is not always the case. The other two cases pertain to the temperature conditions of rocks which are not in accordance with the present mineral alterations in them. There may be cooling whereby the resistivity information will show an overestimate of the temperature distribution compared to the existing condition, or there may be a rise in heat where the resistivity shows an underestimate of the temperature value with the actual one since newer mineral alterations are still building up.

2.2 Resistivity methods

The heat from underneath the earth‘s surface can be utilized effectively by a convection mechanism using a mobile flowing medium and the most abundant material that can transfer this huge amount of energy is groundwater. Hot water interacting with rocks can significantly alter their resistivity. Measuring the resistivity of rocks has been the straightforward means of geophysical exploration work in geothermal prospecting. There are other parameters which aid in any geothermal exploration studies such as temperature and thermal conductivity, the magnetization of rocks, density and seismic velocity but they are not tackled in this report.

Subsurface resistivity data can correlate both with temperature and the alteration of rocks which are key determinants in a geothermal resource study. A number of resistivity methods have been used for

geothermal resource exploration. The oldest one is direct current (DC) measurement but in terms of practicality it is not commonly used nowadays (Georgsson, 2012). The most recent commonly utilized methods are the transient electromagnetic and the magnetotelluric methods. For the purpose of this report, the latter two methods will be discussed.

2.3 TEM theory

The transient electromagnetic method (TEM) is an active method which uses controlled current source to measure resistivity in the ground. The method basically works under two of Maxwell's equations on electromagnetism; one is Faraday's Law which states that the induced electromotive force or the voltage in a closed circuit is caused by the time changing magnetic flux going through the circuit. The other one is Ampere's Law which states that a changing electric field or current would induce a magnetic field around it. Putting these physical laws into geological perspective, the set of conductors where the induced current would flow corresponds to the layers of the earth and the changing magnetic field and magnetic flux corresponds to the effect brought about by Ampere's Law as the controlled current from the loop of wire installed on the earth's surface changes. In mathematical form, we can state the two governing laws of TEM as:

Faraday's law:

$$\oint_{\partial\Sigma} \vec{E} \cdot d\vec{l} = -\frac{d}{dt} \iint_{\Sigma} \vec{B} \cdot d\vec{S} \tag{4}$$

Ampere's law:

$$\oint_{\partial\Sigma} \vec{H} \cdot d\vec{l} = \iint_{\Sigma} \left(\overrightarrow{J_f} + \frac{\partial \vec{\mathrm{D}}}{\partial \mathrm{t}} \right) \cdot d\vec{S} \tag{5}$$

where $\vec{E}; \overrightarrow{J_f}$ = Electric field (V/m); free current density (A/m^2);
$\vec{B}; \vec{H}$ = Magnetic induction (T); Magnetic field (A/m);
$\vec{\mathrm{D}}$ = Electric displacement field (C/m^2);
Σ = Arbitrary open surface with boundary defined by $\partial\Sigma$.

As the controlled current in the source loop at the surface of the earth is turned off, it induces current down into the earth (Figure 3). If the ground is horizontally layered, then the current would flow along these layers as it widens and deepens with time. A series of cylindrical smoke rings centred along the vertical axis of the surface source loop can be depicted to represent the flow of the total current in a given horizontal layer. The area of this loop is generally a simplified representation from the net magnetic flux due to the magnetic field over an infinitely extending earth layer. Each single layer of the smoke ring contributes to an induced magnetic field at the surface at any given time which is dependent on the current density, radius and the depth from the surface (Christiansen et al., 2006). In a more complex earth model where resistivity is no longer horizontally layered, the current rings will then be oriented at different axes and may obtain different geometries deviating away from the shape of the source loop. There is often a sensitivity function which indicates the effective depth of penetration of the smoke rings at certain time periods. This is obtained by summing up the amplitude contributions from the total current density of a layer and

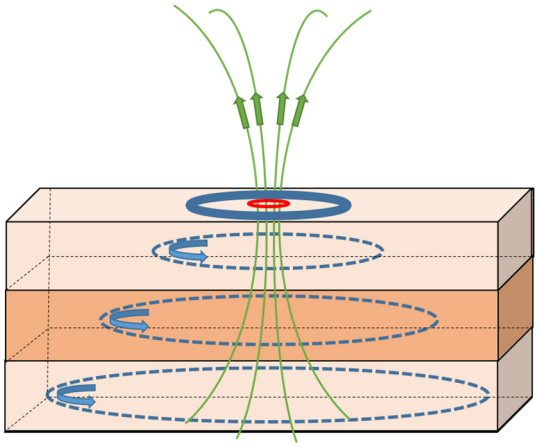

FIGURE 3: TEM working principle where dashed circles represent the net induced ground currents from source loop (dark blue circle on top); green lines represent induced magnetic field which then induces another current in the receiving loop (red circle on top)

the reduced contributions of each of these in every layer as the ground is penetrated. But this depends on the resistivity of the layers since the induced current systems tend to stay longer in conductive layers than do the resistive ones.

The current rings, immediately after the source current at the surface goes down to zero, would decay in amplitude, thus inducing a secondary magnetic field which in turn induces current in any conducting loop nearby. This is how the receiving loop works. The voltage values read by the receiving coil is directly related to the decaying secondary magnetic field from the current rings. At deeper penetration depth, the vertical component of a secondary magnetic field (B_{2z}) at the centre of the source loop can be approximated to be:

$$\frac{\partial B_{2z}}{\partial t} \approx \frac{-I\mu_0^{5/2} a^2 \pi^{-1/2}}{20 t^{5/2} \rho^{3/2}} \tag{6}$$

where I = Maximum current (A);
a = Radius of the source loop (m);
ρ = Resistivity at the penetration depth (Ωm);
t = Time after current turn off (s);
μ_0 = Magnetic permeability in vacuum (H/m).

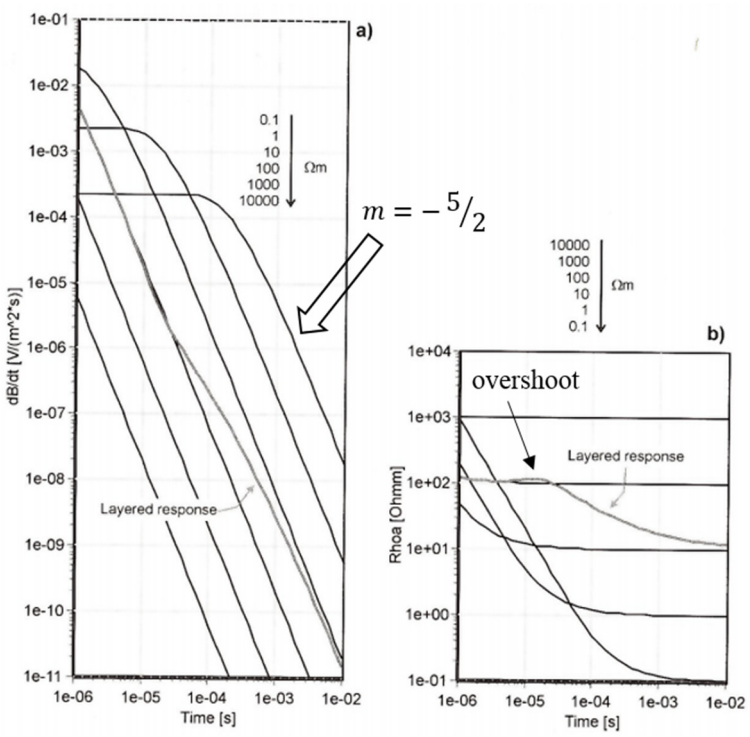

FIGURE 4: a) Impulse responses of the secondary magnetic field with different homogeneous earth models and a sample response of a two-layer earth with 100 Ωm above a 10 Ωm; b) calculated apparent resistivity based on a) (modified from Christiansen et al., 2006)

Equation 6 only simplifies the mathematics involved in obtaining the changing secondary magnetic field i.e. it is only an equation derived by assuming a large value of time (t) where the ratio $\sqrt{\mu_0 \sigma / 4t}$ approaches zero (Christiansen et al., 2006). This now separates the secondary magnetic field response into two major time segments we call early time and late time. This is clearly seen in Figure 4 where early time is approximated with a horizontal line and late time by a negative-sloping line. The equation also tells us that for a homogeneous earth with a source loop having a given current and a constant area, the logarithm of the induced voltage (as related to the time-changing magnetic field) would decay by a constant factor on a logarithmic time scale. Thus, we would expect that at later time, a homogenous earth with different resistivity will have all approaching lines with a -5/2 slope but vertically shifted, i.e. higher resistivity values have lines shifted down compared with the lower ones as seen in Figure 4. We iterate here that at the early time stage of the magnetic field response or equivalently the voltage response, the plot does not in any way reconstruct the real earth layer but only the linear behaviour of the curve and so the apparent resistivity curve starts at an unreliable value at that early stage. Likewise, there is also the unavoidable overshoot of the calculated apparent resistivity from the induced voltage response curve when it shifts from one to the other line with a higher y-intercept, i.e. when the upper layer has higher resistivity than the layer below

it. This overshoot value should not be interpreted as another earth layer. However, this behaviour does not happen the other way around.

Rearranging Equation 6 and using Faraday's Law of induction, we can calculate the resistivity, or properly termed the late-time apparent resistivity, as a function of the voltage of the receiving loop and time:

$$\rho_a \approx \frac{\mu_0}{4\pi}\left[\frac{2\mu_0 A_r n_r A_s n_s I}{5t^{5/2}V(t,r)}\right]^{\frac{2}{3}} \tag{7}$$

where $A_r n_r$ = Effective area: cross-sectional area multiplied by the number of turns of the receiver loop (m^2);
$A_s n_s$ = Effective area: cross-sectional area multiplied by the number of turns of the source loop (m^2);
$V(t,r)$ = Measured induced voltage (V) of the receiving loop as a function of time and radius of the source loop.

The secondary magnetic field is only present when the source current from the loop is turned off. But turning off the source current requires a certain range of time since abrupt current turn off is physically impossible, i.e. it will induce an infinite voltage. In such a time, the receiving loop at the centre of the current loop will create a different signature of electromotive force in the wire depending on whether the current is fully turned off or not. The induced current is exponentially increasing at the time the current approaches zero value but exponentially decreasing from the time when the current is absolutely zero. It is only during the time when the current has been fully turned off that the induced voltage values give a more workable representation of the subsurface resistivity. Thus, turn-off time must be fully determined.

It is also noteworthy to discuss the turn-on effect brought about by switching the current on. In the same principle that the current can never abruptly change, then turning the current on at every instant would similarly create an exponentially increasing electromotive force with opposite polarity. This will linger and may cause additional effect even after current turn off. This is emphasized more as the interval between current turn-on and turn-off becomes shorter, i.e. at higher frequency of the source current.

The actual current source in the transmitter loop is a half-duty square wave with varying input frequencies and signal amplitude. The voltage values are measured after the current is fully turned off. It is read on a logarithmic time scale which is called log-gating (Figure 5). This way, the random noise decreases proportional to $t^{-1/2}$ (Christiansen et al., 2006). The current is cyclic and moves from a

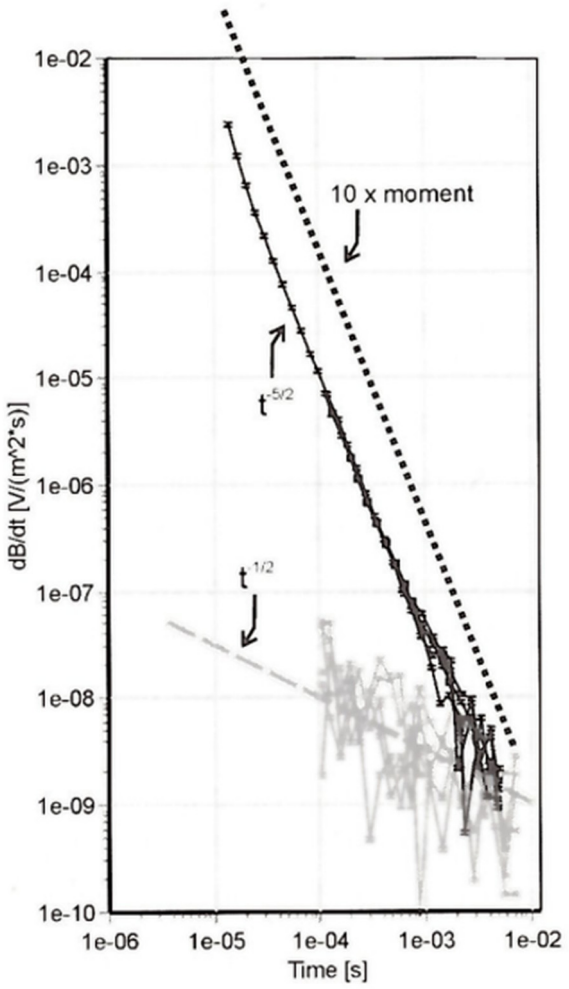

FIGURE 5: Earth response from a TEM sounding (black curve) and the same sounding with 10 times higher moment (dashed lines) with noise level (grey curve) measured in a logarithmic time scale (adapted from Christiansen et al., 2006)

positive current value to a negative one so as to prevent the ground from building up self-potential and thus preventing an unwanted current source. And to be more statistically confident of the measured data and to improve its quality, voltage values are measured and stacked over a number of current cycles. In the same way, increasing the signal source or the magnetic moment of the source loop can help increase the signal to noise ratio. This also helps the late time voltage readings from drowning too much from the noise level.

2.4 MT theory

The magnetotelluric (MT) method is a passive electromagnetic sounding method which uses naturally occurring electromagnetic sources as they propagate into the earth. As these waves penetrate into the earth's material, they induce a current into the ground, called telluric current, which generates secondary magnetic fluctuations. As these two fields are interdependent with one another as expressed by Ampere's and Faraday's Laws in Equations 4 and 5, they are able to delineate the subsurface conductivity as they penetrate into the earth. The transfer function which translates the fluctuation of one field to the other best describes the electrical property of the medium into which they are propagating. MT uses electric and magnetic fields from a period of 0.0025-1000 s and even up to a value of 10,000 s (Figure 6) (Flóvenz et al., 2012). It practically uses two different wave sources. The long period fluctuations of >1 s come from micro-pulsations as a result of solar wind from the sun interfering with the magnetosphere of the earth. The short period fluctuations of <1 s come from lightning activities which are usually generated near the equatorial region of the earth and are distributed throughout the globe via total internal reflection. This source is often called spherics. The period of MT covers, at most, two known ranges having the minimum signal amplitude and are called dead bands. The first one is approximately between the period of 0.0002 and 0.001 s while the other one is between 0.2 and 2 s. The latter has the largest impact for geothermal prospecting since it belongs to the period range where the probed depth usually reaches a hydrothermal resource.

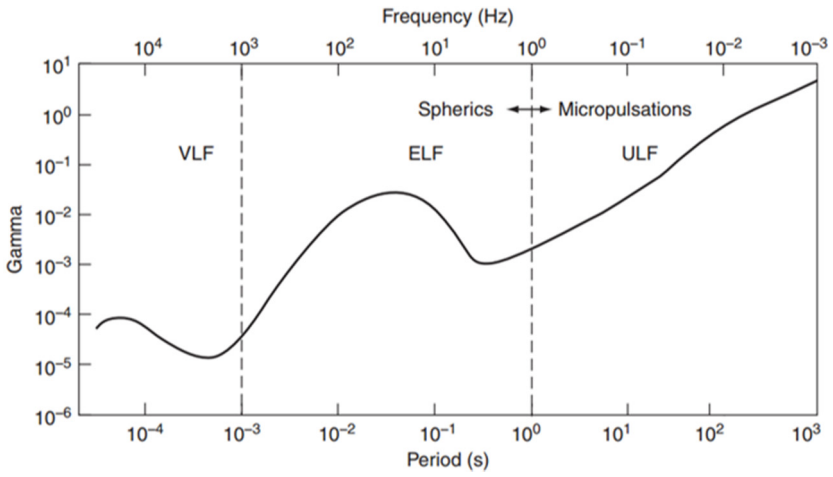

FIGURE 6: Mean amplitude of the magnetic field spectrum which MT uses as a function of period or frequency; note the two local minima of the curve which signify the dead band of the spectrum (from Flóvenz, et al., 2012)

In actual terms, an electromagnetic field is propagating in all directions from its source but behaves more like a plane wave when it gets farther away from it. For simplicity of mathematical computation and analysis, MT assumes electromagnetic fluctuations as plane waves propagating down the earth and since there is a big contrast of refractive index between the atmosphere and the ground, it is likewise simpler to consider that these waves penetrate at normal to the ground surface. Some other assumptions of the earth as discussed by Cagniard (1953) and Keller and Frischknecht (1966) (in Simpson and Bahr, 2005) are considered in MT so as to make calculations straightforward yet acceptable so as not to move far away from the real earth; they are discussed here:

1. The earth absorbs electromagnetic waves but does not generate any or at least in the frequency range where MT works.

2. Accumulation of free charges, specifically at boundary regions, is minimal or not present at all. Otherwise this can mask the actual resistivity value of the earth and can give unreliable interpretations. This is what is known as static shift.
3. The material where MT propagates is entirely ohmic, i.e. the current density passing through a medium is proportional to the electric field present in it.
4. Displacement current is negligible compared to conduction current; and electric permittivity and magnetic permeability do not vary as much as bulk conductivity of the rock material does.

Now, with waves assumed to be uniformly planar in propagation, we demand that both the source electric and magnetic fields be of the form:

$$\left|\vec{V}\right| = \boldsymbol{V_0} e^{i\omega t - \boldsymbol{k}z} \tag{8}$$

where $\left|\vec{V}\right|$ = Electric (V/m) or magnetic (T) field magnitudes;
$\boldsymbol{V_0}$ = Maximum amplitude of both electric (V/m) or magnetic (T) field;
ω = Angular frequency of wave oscillation (rad/s);
t = Time (s);
$\boldsymbol{k}$ = Wave number (m^{-1});
z = Depth (m).

The wave oscillation has to be small enough compared with the earth's curvature so as not to deviate too much from the plane wave assumption and it occurs for electromagnetic signals having a period of less than a day (Srivastava, 1965).

Putting Equation 8 into Equations 4 and 5 (in differential form), we further assume that the source wave is vertically incidental to the earth, i.e. $\partial\vec{V}/\partial x = \partial\vec{V}/\partial y = 0$ and that it is composed generally of linear, isotropic and homogenous media i.e. $\left|\vec{\mathrm{D}}\right| = \varepsilon\left|\vec{\mathrm{E}}\right|$ and $\left|\vec{\mathrm{H}}\right| = \mu^{-1}\left|\vec{\mathrm{B}}\right|$. Then, we can proceed to obtain the equation below:

$$\frac{\partial^2 E_y}{\partial z^2} = i\omega\mu\frac{\partial H_x}{\partial z} = i\omega\mu(\sigma + i\omega\varepsilon)E_y \tag{9}$$

$$\frac{\partial^2 E_x}{\partial z^2} = -i\omega\mu\frac{\partial H_y}{\partial z} = i\omega\mu(\sigma + i\omega\varepsilon)E_x \tag{10}$$

where $H_{x,y}$ = Horizontal components of $\vec{H}$ along 2 arbitrary $\perp$ directions;
$E_{x,y}$ = Horizontal components of $\vec{E}$ along 2 arbitrary $\perp$ directions;
μ, ε = Magnetic permeability (H/m) and electric permittivity (F/m) of a rock material.

For simplicity, it is assumed that conductivity, σ, is much higher by around a factor of ten compared with the electrical permittivity at the highest possible angular frequency (rad/s) i.e. $\sigma \gg \omega\varepsilon_{max}$. Starting from Equations 9 and 10, we can find a unique solution such that the fields will practically diminish to zero when the depth (z) goes to infinity. Finally, we can get the general solution or the transfer function of MT in a 1D earth:

$$H_x = -\frac{k}{i\omega\mu}E_y \tag{11}$$

$$H_y = \frac{k}{i\omega\mu}E_x \tag{12}$$

where k = $\sqrt{i\omega\mu\sigma}$

From Equations 11 and 12, it is straightforward to obtain the apparent resistivity and phase from the complex transfer function. These are expressed in generalized form as:

$$\rho_{ij}(T) = \frac{1}{\omega\mu}\left(E_i^* E_i \Big/ H_j^* H_j\right) = \frac{1}{\omega\mu}(Z_{ij}) \tag{13}$$

$$\theta_{ij} = \tan^{-1}\frac{Im(Z_{ij})}{Re(Z_{ij})} \tag{14}$$

where *i* and *j* stands for any of the *x* and/or *y* components of the electric and magnetic fields.

It is often convenient to express the impedance values in a matrix notation. The conventional matrix form of Equations 13 and 14 is often referred to as the impedance tensor. It represents apparent resistivity and phase values at different orientations in space and at a particular frequency value. We also want to point out another independent tensor called the Tipper vector which shows the relationship of the horizontally propagating magnetic field with the measured vertical magnetic field.

This vector indicates the presence of lateral variations in the ground.

$$\begin{bmatrix} E_x \\ E_y \end{bmatrix} = \begin{bmatrix} Z_{xx} & Z_{xy} \\ Z_{yx} & Z_{yy} \end{bmatrix} \begin{bmatrix} H_x \\ H_y \end{bmatrix} \tag{15}$$

$$H_z = \begin{bmatrix} T_x & T_y \end{bmatrix} \begin{bmatrix} H_x \\ H_y \end{bmatrix} \tag{16}$$

where Z_{ij} = Impedance element at different orientations in space;
T_x, T_y = Tipper vector along $\perp$ and horizontal magnetic fields.

An electromagnetic method such as MT is actually a volume sounding (Simpson and Bahr, 2005). Using the compact matrix form, it is relatively easy to distinguish the geo-electrical dimensionality of the earth as well as to apply the rotation to the values as needed.

In a 1D case as seen in Equations 11 and 12, Z_{xx} and Z_{yy} which are the diagonal components, are always zero, thus, only perpendicular magnetic and electric fields interplay with each other. The impedances from the off diagonal elements of the Z matrix, Z_{xy} and Z_{yx}, have equal magnitude components but opposite signs. It lags a constant value of π for their phases. In terms of the geomagnetic transfer function, or the Tipper, there is no net vertical magnetic effect from the horizontally propagating magnetic fields, since lateral variations in a 1D earth are not present. It is also noteworthy to discuss here that this simplified earth model assumes a rotationally invariant impedance value which may take the form:

$$Z_{det} = \sqrt{(Z_{xx}Z_{yy} - Z_{xy}Z_{yx})} \tag{17}$$

where Z_{det} = Determinant of the impedance matrix in Equation 15.

In a 2D case, the Z matrix can be rotated to a certain angle whereby the diagonal elements are reduced to zero and at the same time maximize the values for both the off diagonal elements. However, in this instance, the latter pair is not necessarily equal. This reoriented Z matrix gives new definition to Z_{xy} becoming the transverse electric (TE) impedance element which runs parallel with the major geo-electric strike in the area as demanded by the 2-dimensionality assumption. The Z_{yx} now becomes the transverse magnetic (TM) impedance element and runs perpendicular to the defined geoelectric strike. It is also important to note from here that the two different impedance signatures should be inverted in a profile direction along with their defined orientations such that profile sections should be made along the geo-electric strike if inverting for TE impedances and perpendicular to the strike if inverting for TM impedances. This dimensionality also demands that the Tipper vector is non-zero along the TE mode, i.e. since it has the magnetic field $H_y$which "sees" the lateral conductivity contrast of the earth. And, thus, the induction arrows, both imaginary and real, orient themselves perpendicular to the strike direction (Figure 7) (Castells, 2006).

In the generalized 3D case, the impedance and the Tipper tensors are all non-zero at any given rotation.

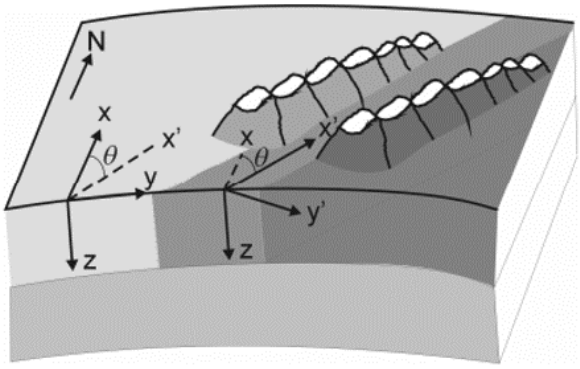

FIGURE 7: Sketch of the 2D dimensionality case of the earth where θ is the rotation of the axis of the impedance tensor from x to x', moving the latter to orient along the strike direction as indicated by surface conditions (adapted from Castells, 2006)

2.4.1 MT penetration depth

The MT resistivity sounding method has the capability of probing very deep, even up to hundreds of kilometres depth (Flóvenz et al., 2012). This depth of penetration is dependent on two variables: the period of the waves and resistivity where the wave is propagating. In a general case, the signal having a longer period can probe deeper. However, the resistivity of the material itself limits the capability of the MT signal to propagate downwards, i.e. if the earth is conductive, the signal tends to decrease at a faster rate than when the earth is less conductive. It is considered that when the signal decreases to 1/e of its maximum value, which is at the surface, then it has achieved its effective penetration depth. In mathematical terms, the skin depth of MT in metres is:

$$\delta(T) = 500\sqrt{\rho T} \tag{18}$$

where T = Period of the propagating electromagnetic wave (s).

2.4.2 Remote referencing

MT data, just like any other geophysical data, are measured with noise. Different types of noises disturb an MT signal but it is usually the coherent noises that are easy to minimize aside from systematic noises. To illustrate, we take one of the extended forms of the element of the Z-matrix defined in Equation 15:

$$Z_{xy} = \frac{\left(E_x H_y^*\right)\left(H_x H_x^*\right) - \left(E_x H_x^*\right)\left(H_x H_y^*\right)}{\left(H_x H_x^*\right)\left(H_y H_y^*\right) - \left(H_x H_y^*\right)\left(H_y H_x^*\right)} \tag{19}$$

where H_x^*, H_y^* = Conjugates of H_x and H_y respectively.

The details of how Equation 19 was derived is not shown here but by assuming that the noise is relatively more significant in the electric than in the magnetic field, we basically add to Equation 15 an error function matrix. By minimizing this error function, we arrive at each of the solutions for the impedance elements like the one shown in Equation 19. It is reasonable to assume that the horizontal magnetic field does not vary significantly from a site to a certain remote location which is usually several kilometres away but only the inherent noises in their respective places. Thus, it is valid to replace conjugates of the magnetic field in Equation 19 with the conjugate values of the equivalent magnetic field at a remote site. Hence, we have:

$$Z_{xy} = \frac{\left(E_x H_{ry}^*\right)\left(H_x H_{rx}^*\right) - \left(E_x H_{rx}^*\right)\left(H_x H_{ry}^*\right)}{\left(H_x H_{rx}^*\right)\left(H_y H_{ry}^*\right) - \left(H_x H_{ry}^*\right)\left(H_y H_{rx}^*\right)} \tag{20}$$

where H_{rx}^*, H_{ry}^* = Conjugates of H_x and H_y of the remote site, respectively.

This eliminates auto powers from reducing the effect from the coherent noises in the magnetic signals of both stations since the uncorrelated noises are now multiplied. As an effect, it reduces the downward tendency of the apparent resistivity curves or the bias, especially at high frequency signals where the stacks are plentiful. The technique discussed was proposed by Gamble et al. (1979).

2.4.3 Static shift problem

MT measurements are done on the surface of the earth. The earth itself has a lot of inhomogeneities which in one way or another alter the path of the telluric currents but not so much as to significantly change magnetic fluctuations. When a field encounters a relatively small shallow body, either resistive or conductive, it changes the value of the electric field at all frequency ranges. This, in effect, multiplies a factor to specific impedance elements as seen in Equation 15, depending on where in space the inhomogeneity is located. In a way, it alters the computed apparent resistivity from this by multiplying it with a constant scalar factor. But this never alters the phase since it is computed as a ratio of the components of the complex impedance. The value of the shift depends upon the contrast of the resistive/conductive inhomogeneity with the surrounding layer. Other means of static shift are caused by changes in topography where the current is redistributed, thus altering the current density and by the presence of lateral structures/boundaries which change the effective voltage drop between measurement poles. All of them contribute to the same effect of vertically shifting the apparent resistivity curves on a logarithmic scale and altering the computed skin depth as well.

However, the reality is that the actual earth layers are not known beforehand. And for the sake of argument, having knowledge of it can always correct for the static shift problem of MT but will defeat the purpose of the survey per se. Thus, at any point in doing the MT survey or even at a processing stage, a geophysicist may not be fully aware of how to correct it, although a lot of computational methods have been proposed to overcome these offsets. One is through spatial averaging at selected frequencies (Bostick, 1986; Sternberg et al., 1982 & 1985; Vozoff, 1990). Another one works out the shift correction with the statistical assumption that the product of the shift multipliers of a large number of MT soundings over a significantly wide area is close to unity (DeGroot-Hedlin, 1991). There is also another study which corrects for static offsets in a sedimentary environment using modal estimates by considering a fixed earth layer at a certain known value (Jones, 1988).

It was pointed out by Árnason et al. (2010) that the DeGroot-Hedlin (1991) assumption was not empirically verified by collating the static shift multiplier values of processed data from Hengill and Krafla in Iceland and the Asal Rift in Djibouti. It was shown that these three cases produced a product of the shift values in the order of 10^{-20}-10^{-10} which are quantities closer to zero than unity. The static shift problem in MT has been its weakness but TEM can effectively correct for the offset. In TEM there are no direct measurements of the electric field from the ground but only through measurement of the voltage produced by induction mechanisms, which is independent of any near-surface inhomogeneity (Table 1).

TABLE 1: Product of static shift multipliers of a large number of soundings in Hengill, Krafla and Asal Rift areas (modified from Árnason et al., 2010)

Area	Number of Soundings	Product
Hengill	149	1.089×10^{-10}
Krafla	124	1.683×10^{-10}
Asal Rift	64	1.045×10^{-16}

2.5 Inversion theory

The apparent resistivity curve is not the actual form of the earth's layered resistivity but only reflects the response of an electromagnetic signal from the layered earth. Thus, through inversion, the apparent resistivity is translated into true resistivity or as close to it as possible. In actual terms, there is no single layered earth solution to an apparent resistivity curve. The uncertainties introduced in the data set give a problem of equivalence whereby combinations of layers' resistivity and thickness values can produce curves that are within the bounds of the uncertainties in the data. In an Occam inversion, which was mostly employed in this report, the approach considers that electromagnetic soundings are not sensitive to sharp boundaries or to significantly thin layers of the earth (Constable et al., 1987).

The inversion works by iteratively adjusting the model parameters such that its forward curve fits well with the measured data. Iteration means that the previous models serve as the basis on how the next parameters should be adjusted based on the fit. As discussed by Árnason (1989), one of the approaches of electromagnetic inversion is by implementing a non-linear least square method whereby the model parameters must be forced to adjust such that the misfit function χ^2 of the response curve against the measured data, apparent resistivity in our case, be at a minimum, i.e. by taking the first-order derivative of all components of model parameters, say j in total, to zero.

$$\chi^2(\boldsymbol{m}) = \sum_{i=1}^{M} [y_i - f(x_i, \boldsymbol{m})]^2 / \sigma_i^2 \tag{21}$$

where $\chi^2(\boldsymbol{m})$ = Misfit as a function of the model parameters;
y_i = Data vector as apparent resistivity (Ωm);
$f(x_i, \boldsymbol{m})$ = Forward response as a function of abscissa variables x_i e.g. time (s) and model parameters $\boldsymbol{m}$ as resistivity (Ωm) and thickness (m);
σ_i = Standard deviation of response values;
M = Number of data points considered in a response curve.

The tedious process of minimization for a non-linear $f(x_i, \boldsymbol{m})$ can be done by iteration. And the process itself needs to have an initial $\boldsymbol{m}$ value which is intended not to move far away from the hypothesized actual earth model. Now, applying minimization to χ^2 with respect to all j model parameters by assuming that the selected model $\boldsymbol{m}$ varies from the actual model by a step value of $\delta\boldsymbol{m}$, then we can say that:

$$\sum_{i=1}^{M} \frac{1}{\sigma_i^2} \left[y_{0i} - f(x_i, \boldsymbol{m}) - \sum_{k=1}^{N} \frac{\partial f(x_i, \boldsymbol{m})}{\partial m_k} \delta m_k \right] \frac{\partial f(x_i, \boldsymbol{m})}{\partial m_j} = 0 \tag{22}$$

where N = Number of partial derivative terms considered in the Taylor expansion of the forward response curve.

From this point, only N numbers of δm are unknown. But the solution is done by implementing the Levenberg-Marquardt method which robustly treats outliers while solving for these small steps in model parameters and updates them every iteration such that this $\boldsymbol{m}$ vector will confidently converge to the empirical or expected value.

3. MEASUREMENT PROCEDURES

3.1 TEM sounding

The central loop TEM measurements are done by placing a loop of wire which is usually a square with a variable area of around 40,000-90,000 m^2 (but can go down to less than 10,000 m^2 for shallower soundings). Alternating half-duty square wave current is applied to the loop with repetition rates that are harmonics of the electrical environment used in the area. This is controlled by the TEM transmitter instrument. The current in the wire can be implemented with an amplitude of around 20-25 A using an electrical generator, but can go to less than 10 A if portable batteries are used. However, we note here that there is a great chance of acquiring data with lower signal-to-noise ratio when using lower current.

Initially, the TEM receiver instrument is calibrated using a known signal source. In the case of Geonics PROTEM digital receiver, a built-in calibration circuit generates an exponentially decaying signal to the instrument that can have four options of time constants and can automate its calibration (Geonics, 1999). Since TEM works with very rapid signal transitions, it is necessary to precisely synchronize the transmitter and the receiver instruments so that the receiver can have the information of the actual turn-off time interval of the transmitter and can start recording from there. Synchronization can come in two

options either by reference cable or by crystal clocks. The two instruments must work at the same repetition rates. Now, a receiving loop is placed near the centre. Different loop areas can be practically used here but the higher the effective loop area, the higher the signal-to-noise ratio of the data gets, especially at late time gates. However, it can be argued here that at higher repetition rates, a smaller loop area should be used to avoid saturation of voltage records. The integration time of the receiver instrument must be taken into account for greater stacking and thus higher data confidence. A particular instance can be illustrated here whereby a 10 m × 10 m square loop with several windings (effective area of around thousands of square metres) is used at a 2.5 Hz repetition rate and another set of measurements using the same repetition rate but with a smaller circular loop of 1 m^2 with 100 windings (100 m^2 effective area). This was done to get quality value of voltage stacks for the later gates using the former set-up and the same for the earlier gates using the latter set-up. In the case of a higher repetition rate of 25 Hz, the same small circular loop was used to acquire good quality data at shallow regions, while the later gates in this case are usually less significant since there is some good overlap with the previous set-up using 2.5 Hz.

3.2 MT sounding

MT measurements are done by setting up perpendicularly oriented electric lines which have electrode pots at the ends, usually composed of lead-chloride with a porous ceramic bottom for measuring telluric currents. The opposite ends must be connected with the N-S and E-W connections in the data logger, although the orientations of these lines might not necessarily follow the cardinal directions. But the choice of it may depend on the terrain or the discretion of the field-man. The endpoints of the electric lines are important and they should be in good contact with the ground. A good strategy is to use a solid water-bentonite mixture as an intermediary between the electrodes and the ground. This is done so that telluric current can easily flow from the ground directly to the measuring instrument or data logger which is commonly placed at the junction point of the telluric lines. A ground electrode is also placed somewhere near the middle or the junction point in order to obtain relative voltage drops for each end of the line and possibly troubleshoot for any anomalous readings. But the ground electrode does not participate in the data collection per se.

Two magnetic sensors, which commonly are elongated coils, should be placed along the orientations of the perpendicular telluric lines. Another coil must be placed normal to the ground. These three coils measure the three independent components of the magnetic field. Hence, they must be stable enough to prevent them from unnecessary movements. This is often done by housing them under a considerable amount of ground which is done by digging. The polarity of these coils must be taken into account and in the case of Phoenix instruments (Phoenix manual), the connected ends of the horizontally oriented coils should face the southern and the western ends of the electric lines as indicated by their connections in the data logger. We note here that the orientation in space of the entire set-up does not matter as long as the relative directions of the component are well established. However, it is a necessity to record the direction of the set-up and the coils used for each line as well as the distances of the electrodes since they will be used for later data processing. The data logger is set to record for at least a day. And it is advisable to acquire data at night-time rather than at daytime since the signal from the former is stronger than the latter (Simpson and Bahr, 2005).

4 GEOLOGICAL SETTING AND PREVIOUS WORK

4.1 Krýsuvík high-temperature area

The Krýsuvík high-temperature area is located on the Reykjanes peninsula, SW-Iceland. As the peninsula is an elevated portion of the diverging Mid-Atlantic Ridge, it has considerable manifestations of post-glacial lava fields with protrusions of hyaloclastites and pillow lavas and breccias, all basaltic in composition (Arnórsson et al., 1975). Krýsuvík area is within the NE-SW oriented volcanic zones

characterized by fissure swarms with intense alteration clays and hydrothermal manifestations like boiling springs and explosion craters. This area along with high-temperature areas in the peninsula deviate from most other high-temperature areas in Iceland, e.g. no indications of volcanic centres are seen (Hersir et al., 2013), but there are indications of intrusions in the base of a buried caldera as argued by Saemundsson in Hersir et al. (2013).

Early exploration studies were done in the area in 1975 (Arnórsson et al., 1975) employing DC measurements as their resistivity method but complications arose in the drilling of exploratory wells. Eventually, MT and TEM measurements were employed in the area in 2007-2008, and then these new data sets were multi-dimensionally inverted into 1D, 2D and 3D cases (Hersir et al., 2010; Lemma, 2010; Hersir et al., 2013).

4.2 Bacon-Manito geothermal project

The Bacon-Manito or Bacman geothermal project is located in the southeast region of Luzon Island which is one of the major islands located in the central part of the Philippines. It is part of the NW-SE trending volcanic belt and is overlain by Pliocene up to younger andesitic and basaltic volcanoes (Panem and Alincastre, 1985). It is situated between two major tectonic zones. To its east is the Philippine trench which is the collision boundary between the Philippine Sea plate and the Eurasian plate. To its west is the Philippine Fault system which runs through the country in a NW-SE direction. The splay of the Philippine fault, which is considered active (Lagmay et al., 2005) in the region of Bacman, is of considerable interest since it affects the structural dynamics in the area. One of them is called the Bacman fault zone (BFZ), predominantly WNW-ESE (Braganza, 2011). Another band lies NW-SE of the region, the Pocdol belt, and has several permeable structures. Likewise, as seen in Figure 8, the region of intersection of the two mentioned zones coincides with the identified and developed geothermal system. Several TEM and MT measurement were done. These data were 2D inverted and a resistivity map of this area has been made recently.

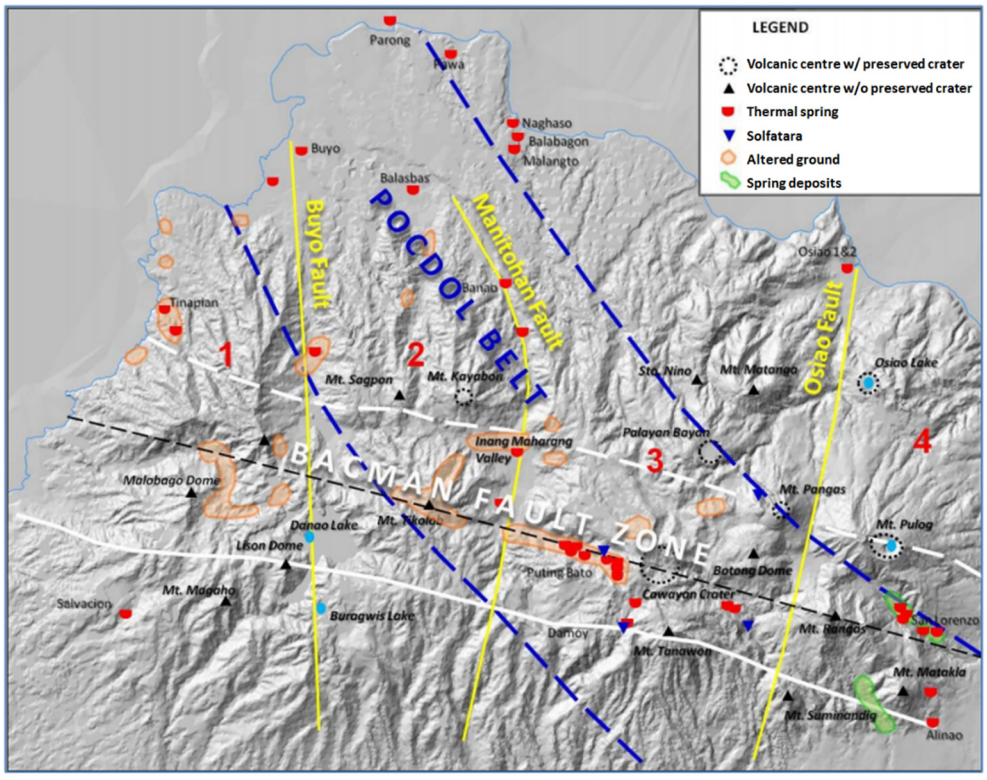

FIGURE 8: Elevation map of the Bacman area with delineated major structures, altered grounds and other thermal manifestations (modified from Braganza, 2011)

5. TEM AND MT DATA PROCESSING FROM KRÝSUVÍK

5.1 TEM processing and 1D inversion

Raw TEM data, which contain the induced voltage values acquired by a 20-gate TEM receiver at different repetition rates of 25 and 2.5 Hz, were inputted into a Linux-based software called TemX (Árnason, 2006a). This was done to convert these values to their equivalent apparent resistivity curves. This graphical-user interface software permits one to remove outlying data points visually. The output format of the files from this software are text files which we conventionally call inv files (since we attach a suffix of .inv at the end).

The inv files were then inputted to an inversion program called TEMTD (Árnason, 2006b). The inversion produces a layered model with resistivity and thickness values for each of the inv files. This program can perform either layered earth or Occam inversion which assumes relatively smoother and continuous resistivity changes of the earth. The latter inversion works with fixed layer thicknesses and assumes numerous earth layers for "smoothness". Additionally, the program permits greater control on the generated models by allowing different constraints to be manually adjusted like smoothness of the model's resistivity, which henceforth is referred to as R (applies the same for layer thicknesses but only used with layered earth inversion), or a damping parameter for regulating oscillation of the model resistivity which from here on is referred to as S (applies the same for layer thicknesses but only with layered earth inversion), a scaling factor for uncertainties in the data, top layer thickness, depth to basement and suppression of some of data points (details in Árnason, 2006b). Inversion was done not only to minimize the misfit but also arrive at an acceptable 1D earth model. An example of an inversion output is shown in Figure 9. It shows an Occam inversion model of 40 layers with R and S equal to 3.2 and 2.6, respectively. A total of 11 TEM sounding data in this area were inverted for voltage values and all resulted in a low misfit value as presented in Appendix I (Africa, 2013).

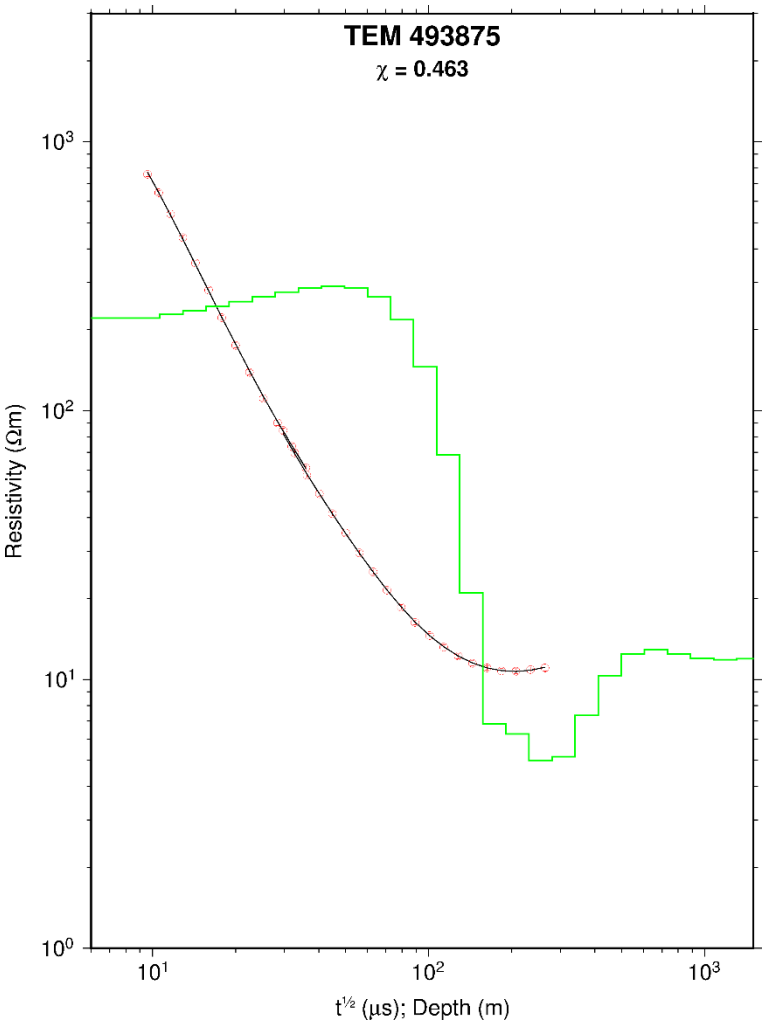

FIGURE 9: 1D inversion results from a TEM sounding; the red dots are the calculated apparent resistivity points from voltage data; the green line shows the layered model generated by TEMTD; the black line is the response from the model

The quality of the fit is one of the best determinants of an inversion output, aside from geophysically assessing the sensibility of the experimental data and the generated model. This is one thing that modern-age computers do well - performing routine minimization. There can be no simpler way to

invert an apparent resistivity curve than by assuming a simple layered earth model by representing the measured resistivity using the minimum possible number of layers. With the data presented in Figure 9, we vary the number of earth layers starting from a three layered earth model until reaching up to less than a hundred layers. We compared the quality of the fit that each of these layered models produced. This was done by successively adding a layer at every turn of inversion starting from the simple 3 layered earth. The previously generated model was used as the initial model for the next run until reaching the highest attainable number of layers. The procedure was implemented under a constant set of parameters, i.e. 5 iterations per Occam inversion with a basement depth of 1000 m, top layer thickness of 5 m, R and S were equal and the rest of the parameters were set as default.

The plot in Figure 10 generally shows a decrease in the misfit value as the number of layers is increased. For all three cases of R and S values, curves were observed to significantly relax and gradually decrease in misfit after around 30 layers. In the case where R and S parameters were not considered, i.e. both R and S were zero, the misfit approached its minimum with a lower number of layers than in the case when R and S were non-zero, especially when they were both set to 10. This suggests that having more layers in the model can more easily make the inversion approach a better fit but adding constraints to the model limits its freedom to allow equivalent models to be noticed, thus hampering fitting or making the misfit higher. Given reliable data, a model with low misfit values may not necessarily be acceptable, but an acceptable model should always have a low misfit. In the end, the choice of an acceptable model relies on the discretion of the geophysicist.

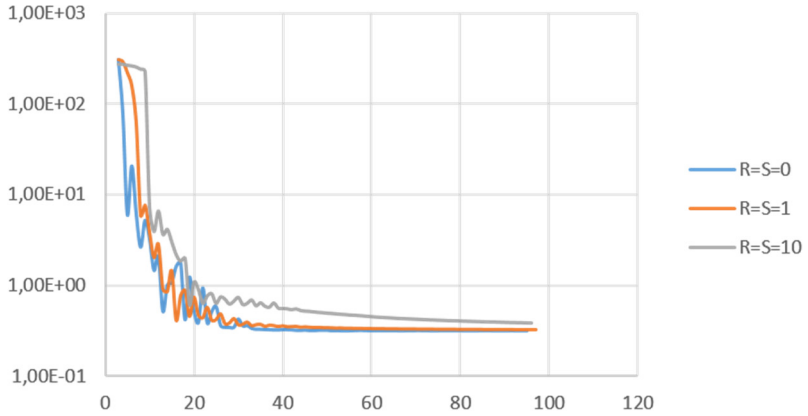

FIGURE 10: $\chi 2$ misfit value of the forward response with the measured data as a function of number of layers of the model; plots were obtained from inverting a single TEM sounding data using constant parameters but only varying resistivity smoothness and oscillation

5.2 MT processing, static shift and joint 1D inversion

Raw MT data are time series data containing two electric and three magnetic field readings (if a 5 channel set-up is used) at 3 different sampling frequencies to serve as low-pass filters and sampling intervals to serve as high-pass filters. These data are inputted to the software provided by Phoenix Geophysics (as we are using their manufactured MT instruments) in order to convert these time series values to auto- and cross-powers where impedance, Tipper, coherency, Z-strike, skew and other desired values are embedded. This is implemented first in SSMT2000 by segmenting the series and applying Fourier transformation to extract the frequency components of each segment, remote referencing the calculated values of the overlapping segments and applying robust estimation. The rest of editing is visually done using the graphical-user interface software called MTEditor where unwanted outliers are further removed from the data. The final output file is called an EDI file where EDI stands for electrical data interchange (SEG, 1991).

From the EDI files generated, it is recomputed to obtain the needed impedance values or the apparent resistivity and phase and the strike. Since we are processing data in a 1D dimension case, then only the determinant of the impedance tensor is used to make it rotationally invariant.

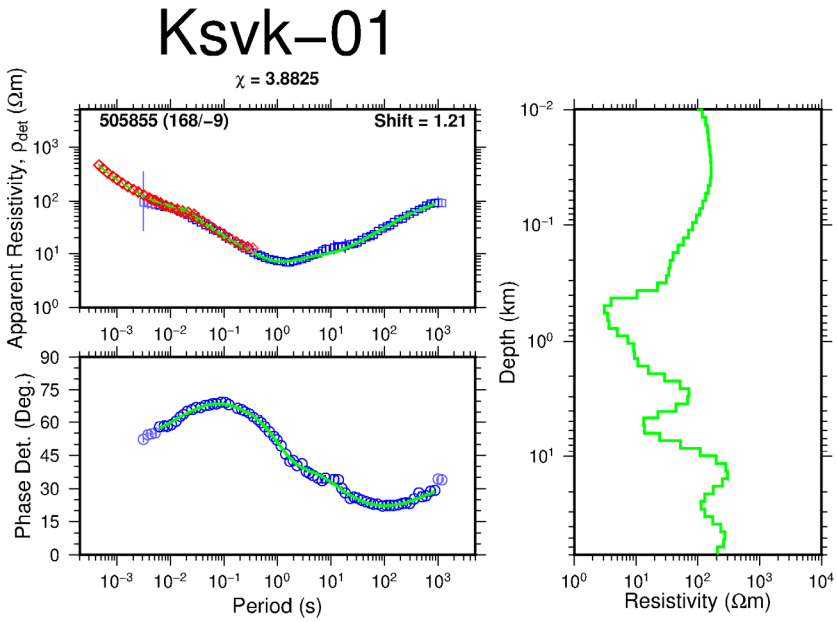

FIGURE 11: 1D joint inversion result of TEM and MT sounding; red diamonds are TEM apparent resistivity points transformed to pseudo-MT points; blue squares are MT apparent resistivity and blue circles are MT apparent phase points which are derived from the determinant of MT impedance tensor; Green lines on the right represent 1D joint inversion model and on the left represent the model´s MT apparent resistivity and phase response. The name on top of the plot is the MT station name with the misfit value of the model; the data is given by the equation below it. The shift value implemented to MT data so that it would fit the TEM data is 1.21. The name of the TEM sounding is 505855 with an aerial distance of 168 m from the MT sounding and elevation difference of 9 m

After calculating and editing the apparent resistivity curves for both the TEM and MT, they are ready for joint inversion. This was implemented using TEMTD software but this program can also do inversion of TEM or MT separately. TEMTD considers the MT apparent resistivity shift as part of the parameters that is inverted for, although "force shifting" was also possible. Figure 11 shows a sample of the best fitted model, where the data were inverted for voltage of the TEM data, and for the apparent resistivity and phase of the MT data. Unwanted data points were disregarded in the inversion. All data were inverted using Occam inversion method with varying first and second order derivatives of the resistivity layers such that the model will be optimized for resistivity smoothness and avoid unnecessary oscillations in their values. Looking closely at Figure 12, we see that the fit of the response goes well with the measured data but a slight off is seen in the period range of around 10 s. This could be due to the 3D behaviour of the impedance data at that particular period range.

5.3 Sensitivity-to-depth test

MT penetration depth can be best approximated by skin depth as seen in Equation 18. Here we test the sensitivity to depth of a joint TEM and MT sounding in Krýsuvík. First, depth to basement was reduced to around 6 km as modified from the best generated model having a depth of 45 km. This new model was inputted as an initial model in the joint inversion with all other parameters kept the same as with the best model. Figure 12a shows the result. It produces an acceptable fit with a chi square value of 4.84. The best model generated a misfit of 4.79 which gives a very close value with the shallower model. In the second case, depth to basement was cut to a shallower depth of around 5.1 km as modified from the same best model. Inversion results as seen in Figure 12b give a model with a significantly larger misfit of 10.30 from the initial 4.79. The response noticeably misfits the highest frequency periods of the data as expected. It means that at this depth range of 5-6 km and for this particular sounding, there is a significantly high sensitivity in the fitting capability of 1D joint inversion, especially at the highest frequency points of the MT data. However, extending further down from this basement depth of 6 km can result in a slightly better fit, but the reliability of the resulting model below 6 km is another thing to look at.

5.4 Model results

A total of 21 MT sounding data and 20 TEM sounding data were jointly inverted, meaning two MT stations used a single TEM sounding. This data set produced two profiles cutting SE-NW through the survey area. Three boreholes with hydrothermal alteration data were used on the profiles. Figure 13 shows the map of the Krýsuvík high-temperature area together with the location of the TEM and MT soundings as well as the profile trace generated from them.

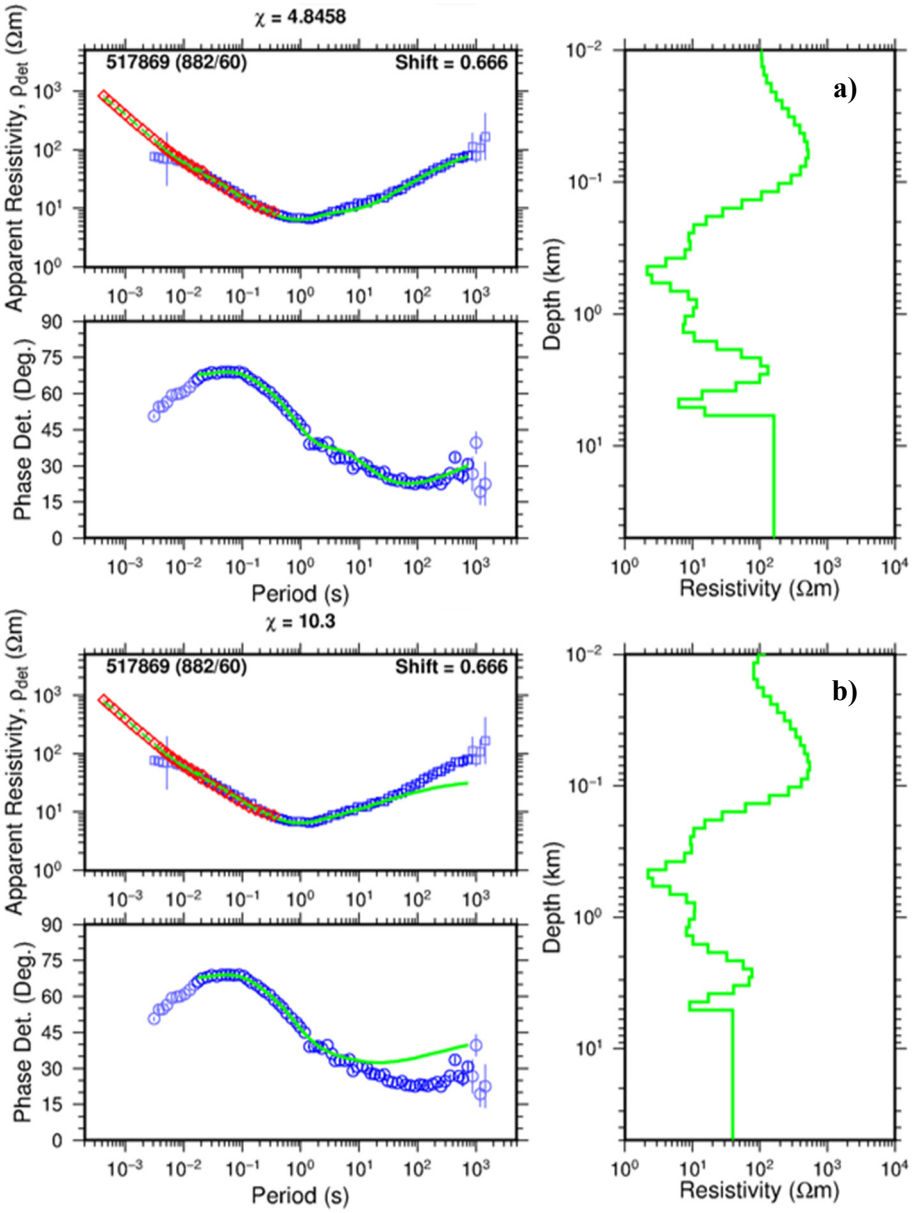

FIGURE 12: In a) basement depth of the best model was reduced to 6 km; this initial model produced an inversion result with 4.84 as misfit; b) basement depth of the best model reduced to 5.1 km which produced a result of 10.30 as misfit

The two profiles run from NW-SE and cut through the fissure structures. The profiles shown in Figure 14 extend down to 10,000 m below sea level; these same profiles are shown in Figure 15 at a shallower depth of 2000 m below sea level. Both of the profiles exhibit low resistivity values of <10 Ωm at shallow depths of up to around 1500 m, but deepen considerably at the southeast end of profile 2 and the northwest end of profile 1 which are seen farthest from the fissure swarms. Updoming configuration of the low resistivity region is pronounced in the central region of profile 2. The defined low resistivity zone can be interpreted as rocks having extensive amounts of low-temperature secondary alterations like smectite or zeolite. The moderately high resistivity of less than a 100 Ωm, as seen underneath the low resistive cap, suggests the presence of secondary alterations like chlorite and epidote. The presence of some highly resistive regions of around 200 Ωm below the identified clay cap (mostly seen on profile 1) is most probably related to impermeable rock regions where lesser amounts of groundwater can come into contact, thus maintaining its high resistivity characteristic compared to its immediate surroundings. The surface and near-surface high resistivity regions of several hundreds of Ωm in value are represented by the young volcanics covering the region which are fresh unaltered rocks and mostly above the water table. Low resistivity values are also seen close to the surface where fumaroles are located.

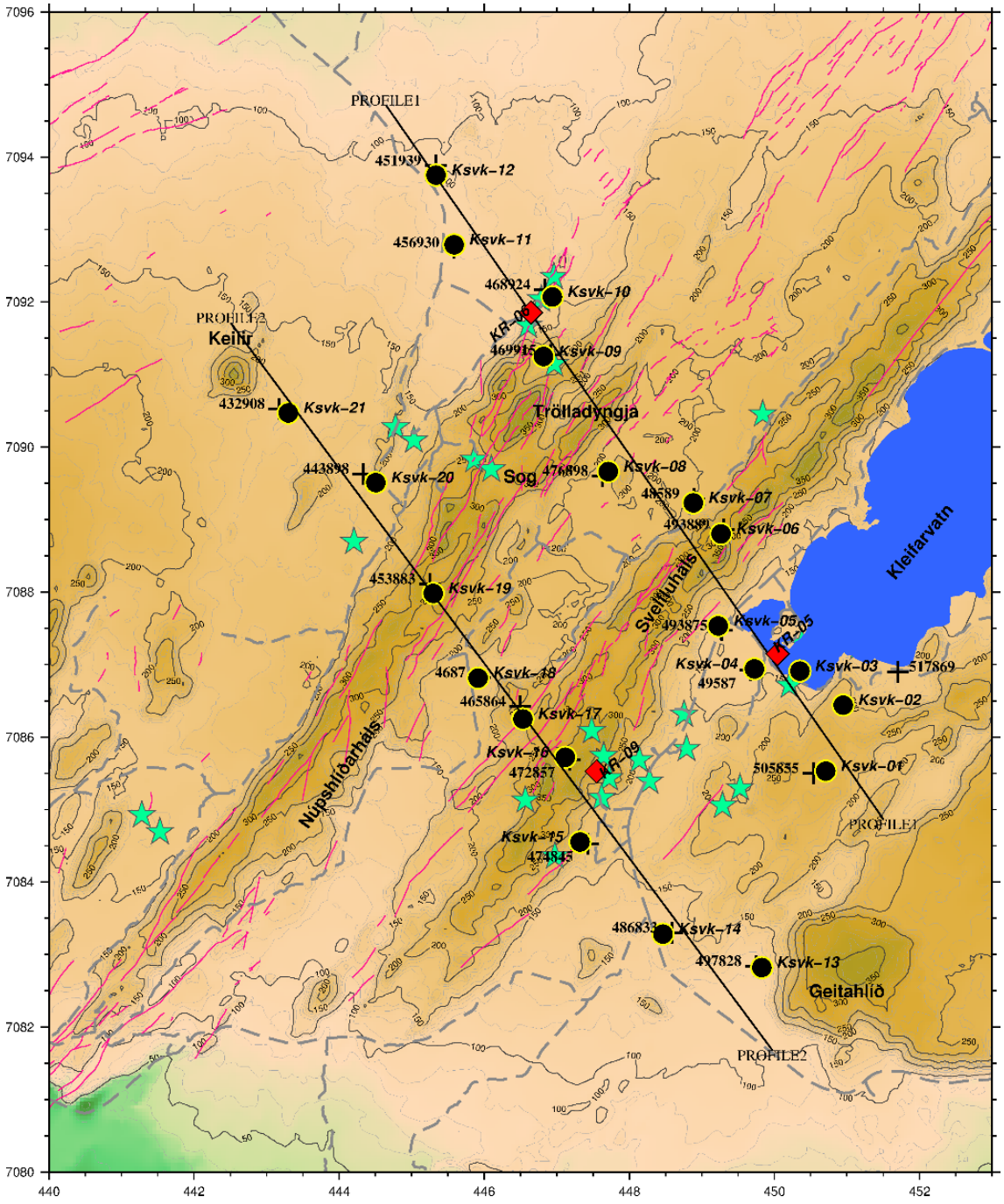

FIGURE 13: Map of Krýsuvík high-temperature area, SW-Iceland; shows locations of MT soundings represented by black dots, TEM soundings by crosses, fumaroles by green stars, boreholes by red diamonds and identified faults by red lines

The two profiles also intersect three wells. Well KR-05, at around 820 m depth, intersects profile 1. In it, chlorite alteration is found at around 100 m depth. In well KR-06, smectite-zeolite alteration is found between 50 and 450 m depth and chlorite is dominant from 450 down to 840 m which is the final depth of the well (Hersir et al., 2010, and references therein). There is quite a good correlation of smectite as it is mostly found within the decreasing resistivity of the region, having values of less than 6 Ωm. The chlorite below it overlaps well with the increasing resistivity. There seems to be a good correspondence between the dominant alterations in the wells with the resistivity structure of the profile. However, looking at the well temperature data, the system suggests fossil alteration since the rock temperature

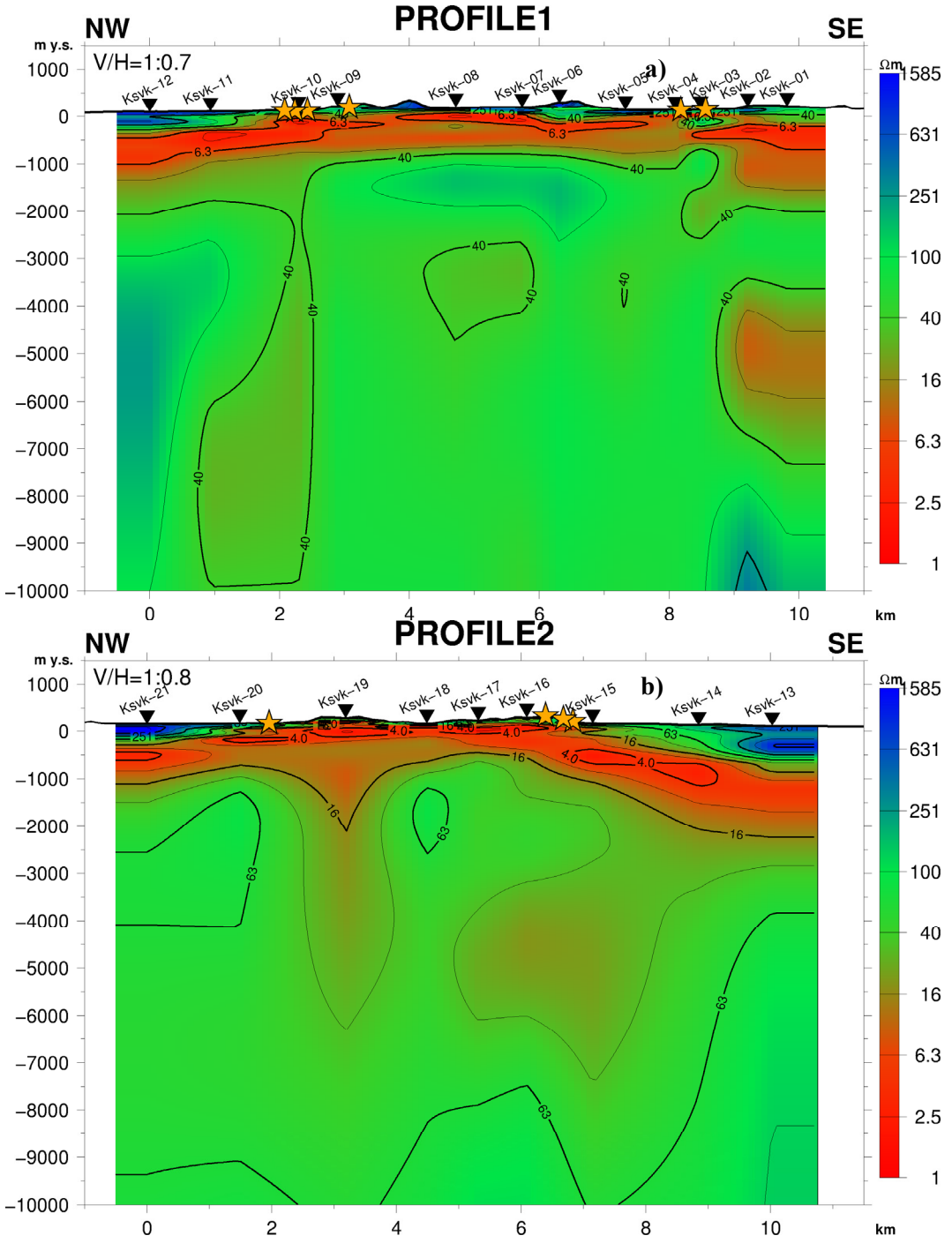

FIGURE 14: The 11 km long a) Profile 1 and b) Profile 2 both cutting NW-SE through the region of Krýsuvík; inverted triangles on the surface are MT stations and orange stars are intersected fumaroles; locations of these profiles shown in Figure 13

shows lesser values than the expected formation temperature of the alteration minerals. There is also an evident temperature inversion in the system.

Well KR-09, at around 330 m in depth, intersects profile 2. A smectite-zeolite zone found at the top 130 m depth of the well intersects with the identified low-resistivity cap. Mixed clay from 130 m down to the final depth of the well is seen and overlaps the increasing values of the identified low-resistivity cap (Hersir et al., 2010, and references therein). However, values of <10 Ωm are considerably low for the existence of mixed clay alterations. This may still be reasonable since this well is around 400 m away from profile 2.

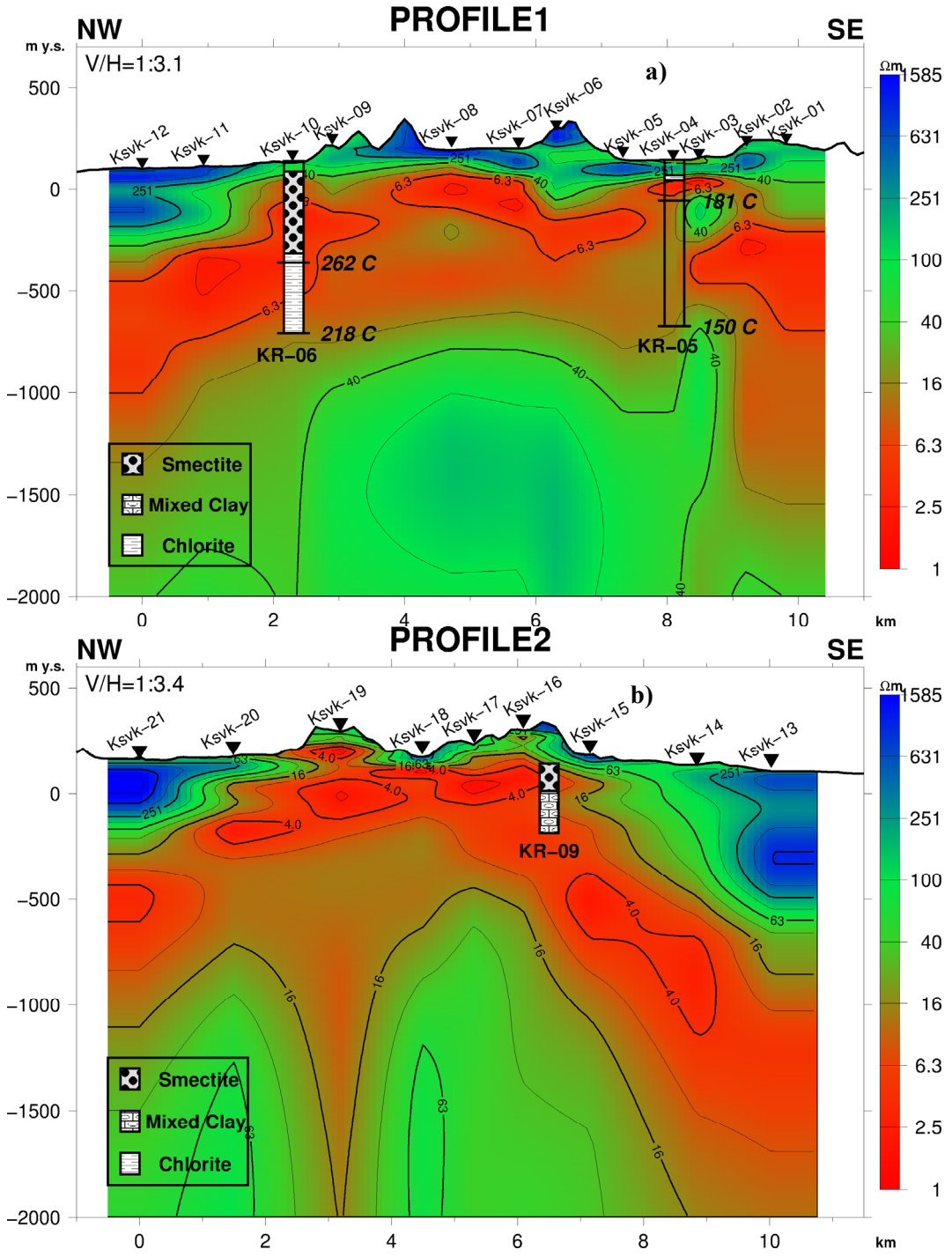

FIGURE 15: a) Profile 1 and b) Profile 2 shown down to 2000 m depth with nearby wells projected into them; good correlation of resistivity seen with indications of alteration minerals in both profiles which mostly intersects the observed low-resistivity cap: locations of profiles is shown on Figure 13

In terms of the shift offset of the MT apparent resistivity data, it can be observed that most of them are shifted down by a factor between 0.5-0.9 as seen in the histogram plot in Figure 16. Looking at the corresponding distribution of the shift on the contour map in the same figure, it can be observed that the area where down shifts occur are mostly found within the region where a lot of thermal manifestations are located. This is a good confirmation of how static shift is affected by shallow resistivity inhomogeneities whereby, in this scenario, low-resistivity alterations from surface thermal manifestations shift MT apparent resistivity down to a lower value.

The Tipper strike from different period ranges was obtained. It can be observed from the rose diagram of the T-strike at a period range of 0.01-0.1 s in Figure 17a that there is a significant resistivity contrast along the NW-SE direction at a very shallow depth. Some of the soundings do not show T-strike information since there was no vertical component magnetic sensor installed during data acquisition. This alignment is consistent with the presence of the shallow low resistivity seen in the central region of profiles 1 and 2 which happens to coincide with the locations of the fissure structure. It is clearly shown by the real component of the Tipper arrow at 0.05 s period as shown in Figure 17b. As these arrows point away from conductive bodies, there are apparent indications of low-resistivity structures lying within the fissure system.

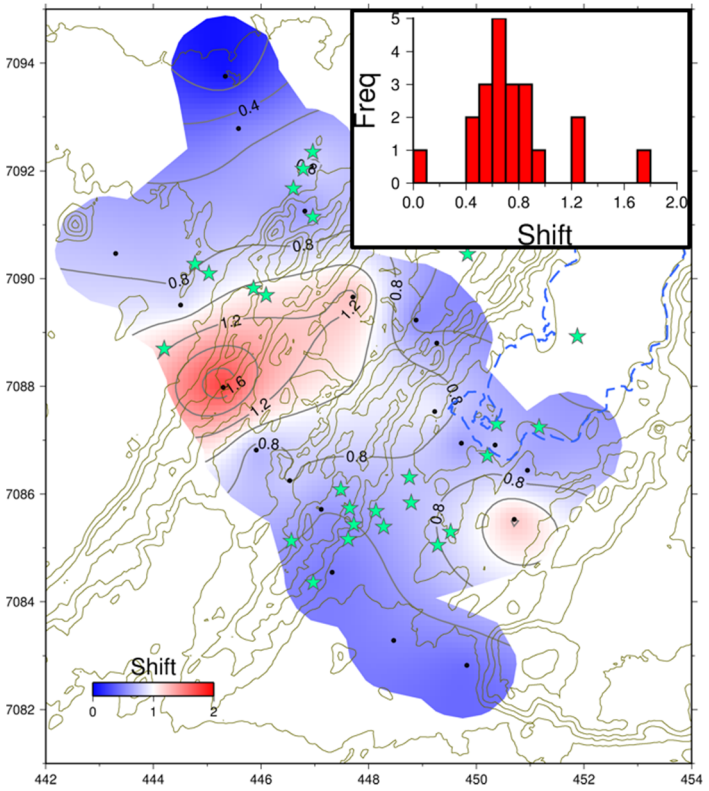

FIGURE 16: Shift histogram of all the inverted MT soundings in Krýsuvík with their contoured values overlain in a topographic map; shift values of less than unity are found within the regions where thermal manifestations are located

Looking at greater depth corresponding to an MT period range of 10-100 s, T-strike starts to align well with the sea water located immediately south of the area, as seen in Figure 18a.

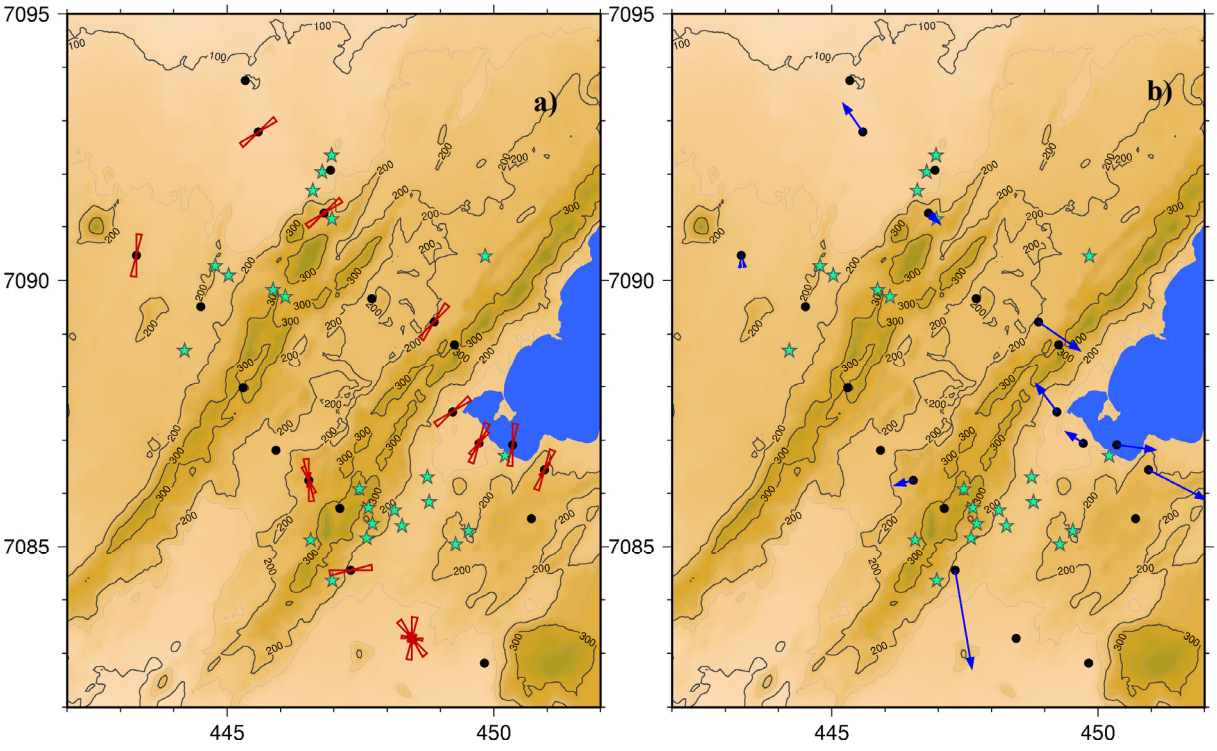

FIGURE 17: a) Tipper strike between period range of 0.01 and 0.1 s; b) real part of the induction arrows at period of 0.05 s

The presence of the highly conductive sea, with an average resistivity of 0.3 Ωm, makes the real component of the Tipper arrow point away from it (see Figure 18b). The shallower and more resistive fresh water from the lake is negligible.

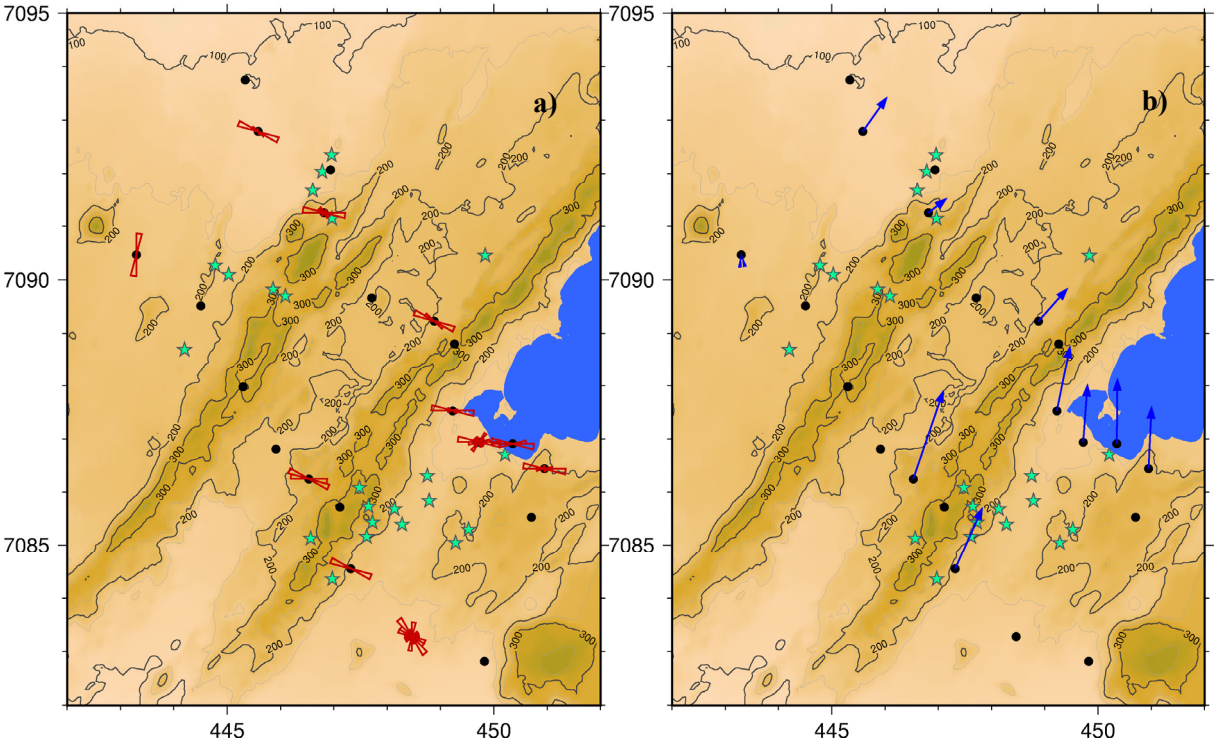

FIGURE 18: a) Tipper strike between period range of 10 and 100 s;
b) real part of the induction arrow at period of 30 s

Due to the 90° ambiguity of the Z-strike, it is more often reliable to assess lateral resistivity variations using the Tipper information. This is another independent data set which relies on the relationship of the vertically changing magnetic field with the horizontally oscillating magnetic fields as shown in Equation 16 which, in a way, confirms the resistivity structure produced by inverting the apparent resistivity and phase values of MT derived from the transfer function (impedance tensor in Equation 15) relating the horizontally oscillating electric and magnetic fields.

6. REVIEW OF RESISTIVITY DATA FROM BACMAN

Over a hundred MT and TEM soundings have already been done in BacMan area. Joint inversion for several soundings was not possible due to the poor overlap of TEM with the MT data. In this report, only 10 pairs of MT and TEM sounding data were considered for inversion. Figure 19 shows the location of some of the MT and TEM data in the area with the three sections considered in the joint inversion.

6.1 TEM inversion

TEM data were collected using the Geonics PROTEM 47D system under 60 Hz at the survey area; the country, as a whole, uses the same power line frequency. The transmitter instrument generated current with repetition rates of 285 and 75 Hz and maximum current of 2-4 A. The transmitter loop was set-up to a 40 m × 40 m area. The soundings were done in two configurations: in-loop and out-loop. A current of 2 A was deployed in an in-loop configuration while a current of 4 A was deployed in an out-loop

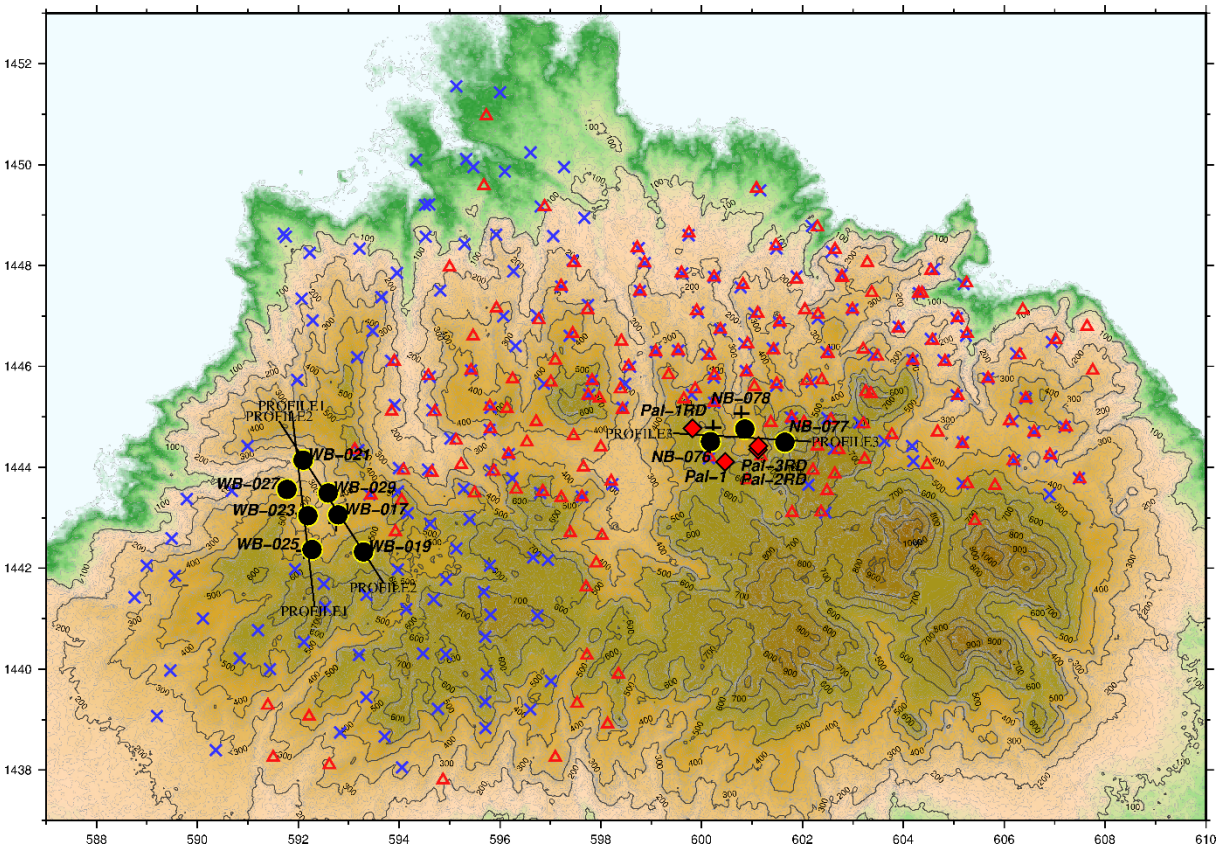

FIGURE 19: Map of Bacon-Manito geothermal area; black dots and black crosses are the inverted MT and TEM sounding data, respectively, with profile lines shown running across these points; red diamonds are location of some wells in the area; blue crosses are MT and red triangles are TEM soundings done in the area (but not processed in this report)

configuration. However, the TemX program only calculates the apparent resistivity data from an in-loop configuration of TEM. Thus, processing and inversion was done using the in-loop TEM data only. At this point, it is noteworthy to point out that in terms of the calculated apparent resistivity, the in-loop and out-loop TEM configurations will have different signatures at early measurement times but will virtually converge at later times. This is caused by the presence of different orientations of the secondary magnetic fields inside the offset loop when the smoke rings are in the early and shallow stage, but at late and deeper propagation, the expanded smoke rings will consider the offset receiver to be almost identical with the in-loop receiver, i.e. the secondary magnetic field is passing through these loops with similar orientations, i.e. vertically when the earth has very small or no lateral resistivity variations.

Several of the TEM soundings have low signal-to-noise ratio since low current amplitude of 2 A was used and little data stacking was done. Since the decay falls off in the order of $t^{-5/2}$, then small amplitude signals can easily be drowned in noise after a short time. Out of these, a number of good TEM soundings were inverted and compared. Using the set-up described above, sounding depth reliably reaches up to around 200 m. This shallow profiling can well resolve the upper layer resistivity of an area. However, for the purpose of geothermal exploration, resolution of shallow earth is usually not considered significant. The very shallow resistivity structure of the earth is usually not observed when a lower frequency of the source current is used since this earth layer is seen at its early time measurements and normally shows a shoot up response in the apparent resistivity. There may also be the possibility of coupling of several of the poor quality TEM data which made the data points oscillate or deviate from the true value even after multiple stacking (Christiansen et al., 2006). This problem causes a large deviation of the inverted model from the actual earth structure if not considered beforehand since it may also represent an undisturbed response. But there can be no straightforward means of validating the sounding unless obvious evidence of the source of noise is recognized in the field or a tightly spaced

TEM sounding is employed. Figure 20 shows the measured apparent resistivity of two different areas in BacMan. A good fit was established for both of the soundings. The entirely different shallow resistivity profiles produced from the inversion may suggest different local resistivity conditions in the area. Significantly, the increasingly deeper end of the apparent resistivity seen in Figure 20b may suggest two possibilities for the model at deeper levels, i.e. higher resistivity is present below the lower one as shown in the generated model or an even conductive layer is present below the resistive top layer similar to what was shown in Figure 4b.

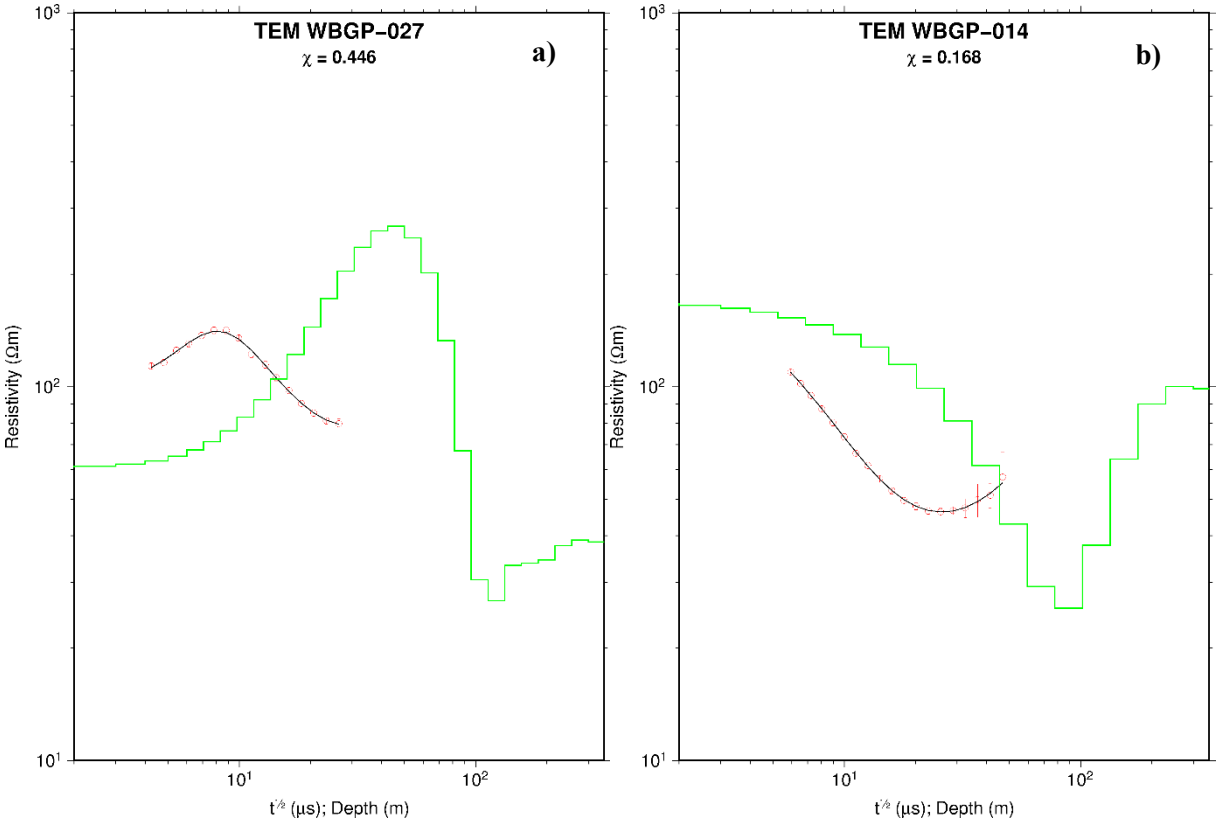

FIGURE 20: Sample of the inverted TEM data in Bacon-Manito area; soundings were inverted up to a basement depth of around 300 m

6.2 MT and TEM joint inversion

1D joint inversion, specifically TEMTD, considers the MT shift value as one of its unknown parameters such that the generated model is able to fit exclusively both TEM and MT data. Hence, a considerable number of overlapping TEM and MT data points must be present in order to have a reliable joint inversion. The high frequency apparent resistivity of MT data may usually have downward bias even after remote referencing since this only reduces the effect of coherent noise. TEM data, which in our case only considers induction from the vertical secondary magnetic field, may see lateral resistivity or 3D effects and display the deeper end of the apparent resistivity curve up which overestimates the actual resistivity value since the horizontally measured induced voltage is always less than the actual one (secondary magnetic field is no longer perpendicular to the surface). But it should also be pointed out that the same behaviour can be observed if the earth is 1D only if the horizontal components of the secondary magnetic fields are almost zero. In the end, distinction from this effect is often difficult unless non-horizontally induced voltages are measured. These two independent issues of the methods may result in an unreliable calculation of the shift parameter or even fitting if few overlapping points are established. One particular instance is shown in Figure 21. Figure 21a shows a case of inverting MT and TEM data where the program looked for the most probable shift parameter such that the misfit was

at a minimum. We can observe that the model produced a response where late time points of TEM and the high frequency of the MT do not overlap. Here, the program tried to find a model that could satisfy the linkage between TEM data with MT data curve as dictated by the phase information which anticipates the resistivity behaviour at a shallower depth where TEM is supposed to coincide. Figure 21b shows the inversion result of the same data set where the MT shift value was fixed and the scaling factor was set to a higher value so that the response could have a larger range of values to play around with as iteration proceeded. There is an observed overlap of points between the MT and TEM data but since the high-frequency phase data sees a higher value of resistivity at shallower depth, it forces the response curve in the TEM range to shoot up. Figure 21c shows the inversion result of the force-shifted MT data but with less of a leeway range for the response, i.e. allowable models are more restricted than the previous one. The result is a good overlap of the response with the apparent resistivity curve of both MT and TEM but a poor fit with the high-frequency phase points as expected. It can be noticed that the three models produced significant changes in resistivity values at depth corresponding to the junction region of these two data. Hence, a deeper TEM sounding with a considerable overlap with the MT data could possibly improve the reliability of the inversion results.

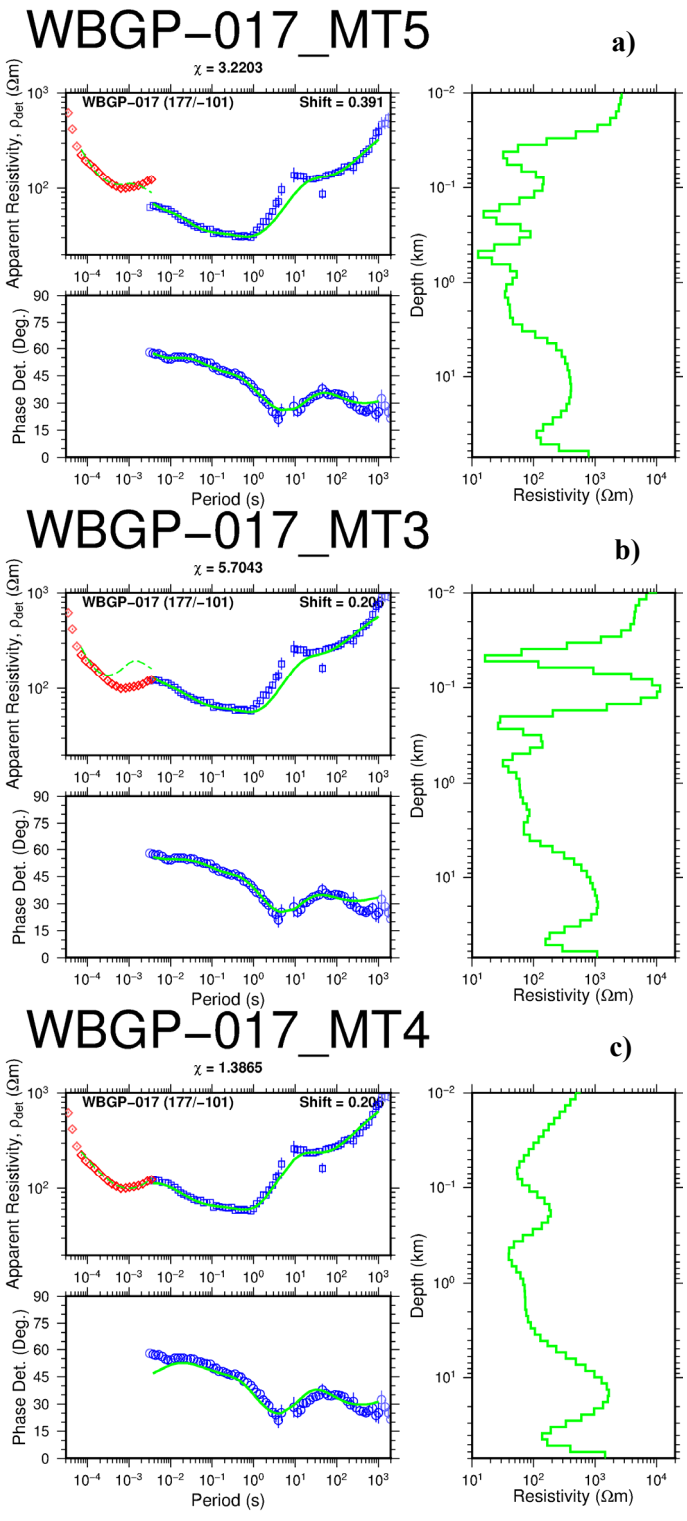

FIGURE 21: Three cases of joint inversion results: a) Shift parameter was determined by the program; b) Shift parameter was set by used with high scaling factor for data uncertainty; c) Same as b but scaling factor is further reduced

Now, we look at the profiles generated in the western part of the area as seen in Figure 19. It can be observed that the near surface resistivity extending down to 1500 m depth has a low-resistivity signature from around 10-20 Ωm. This is prominently seen on profile 1 (Figure 22a), less so on profile 2 (Figure 22b). This low resistivity can be associated with a highly loose or scattered mineral alteration since the area where the section is located has a considerably altered ground but no thermal springs, as shown in Figure 8. The water table might also contribute to lowering the resistivity structure at shallow layers of both profiles. A relatively elevated water table in this area can be inferred from the nearby Danao Lake (shown in Figure 8) which is located on the southeast end of these sections and has a surface elevation of roughly 400 m above sea level. The highly resistive signature on the

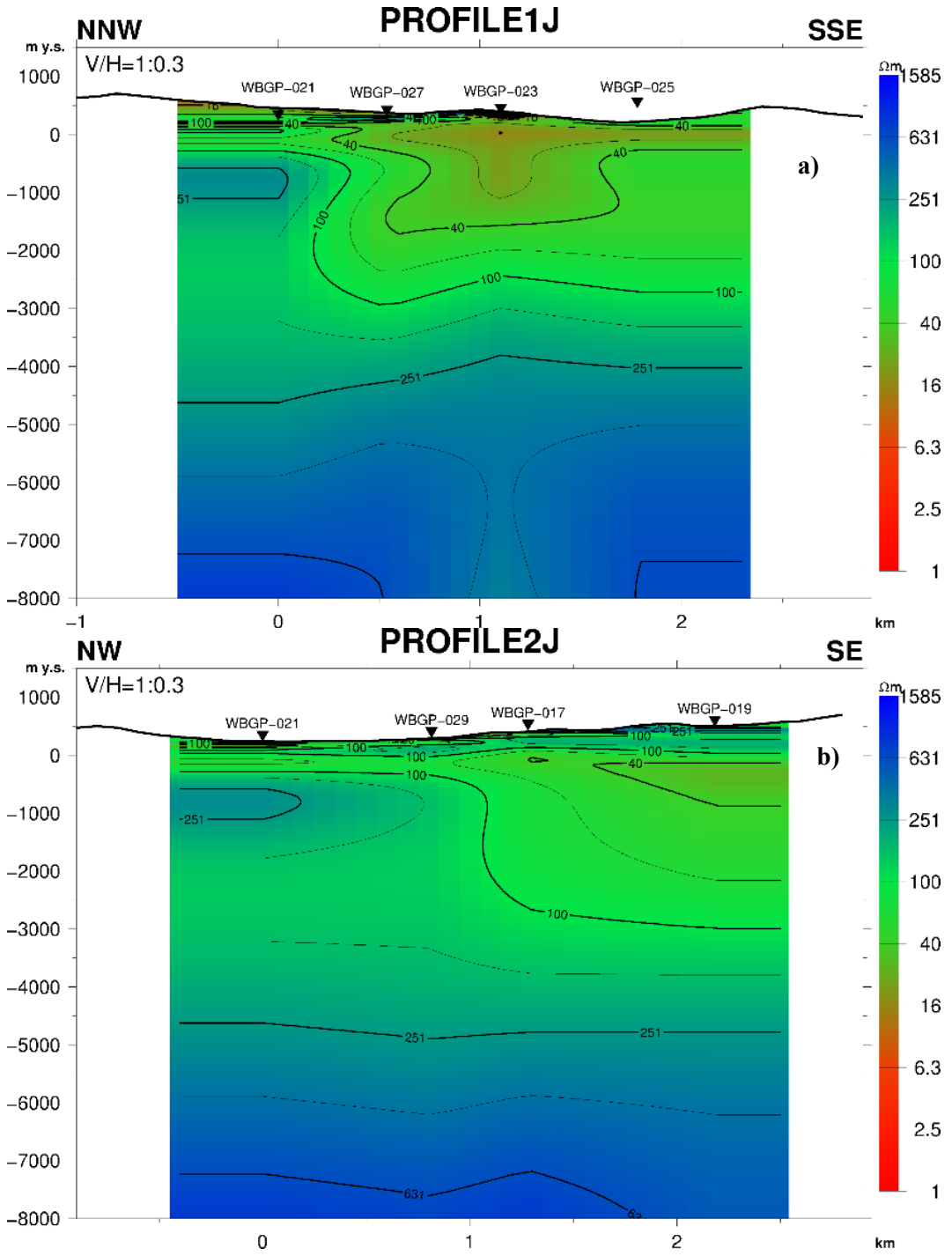

FIGURE 22: Jointly inverted 3 km a) profile 1 located on the far western part of Bacman geothermal project running NNW-SSE, and b) profile 2 located also on the same part of the area running NW-SE and intersecting profile 1 at the northwest end (see Figure 19 for location)

northwest side of both profiles suggests the presence of unaltered and possibly less permeable structures since we take notice that this end of the profile is nearest to the sea and it could have an extensively low resistivity value if this end was permeable. The very resistive layer at the bottom can be interpreted to be another impermeable rock structure, the Manitohan volcanic centre, which may be part of the oldest volcanic system in the area (Braganza, 2011). This may indicate part of the western periphery of the geothermal resource.

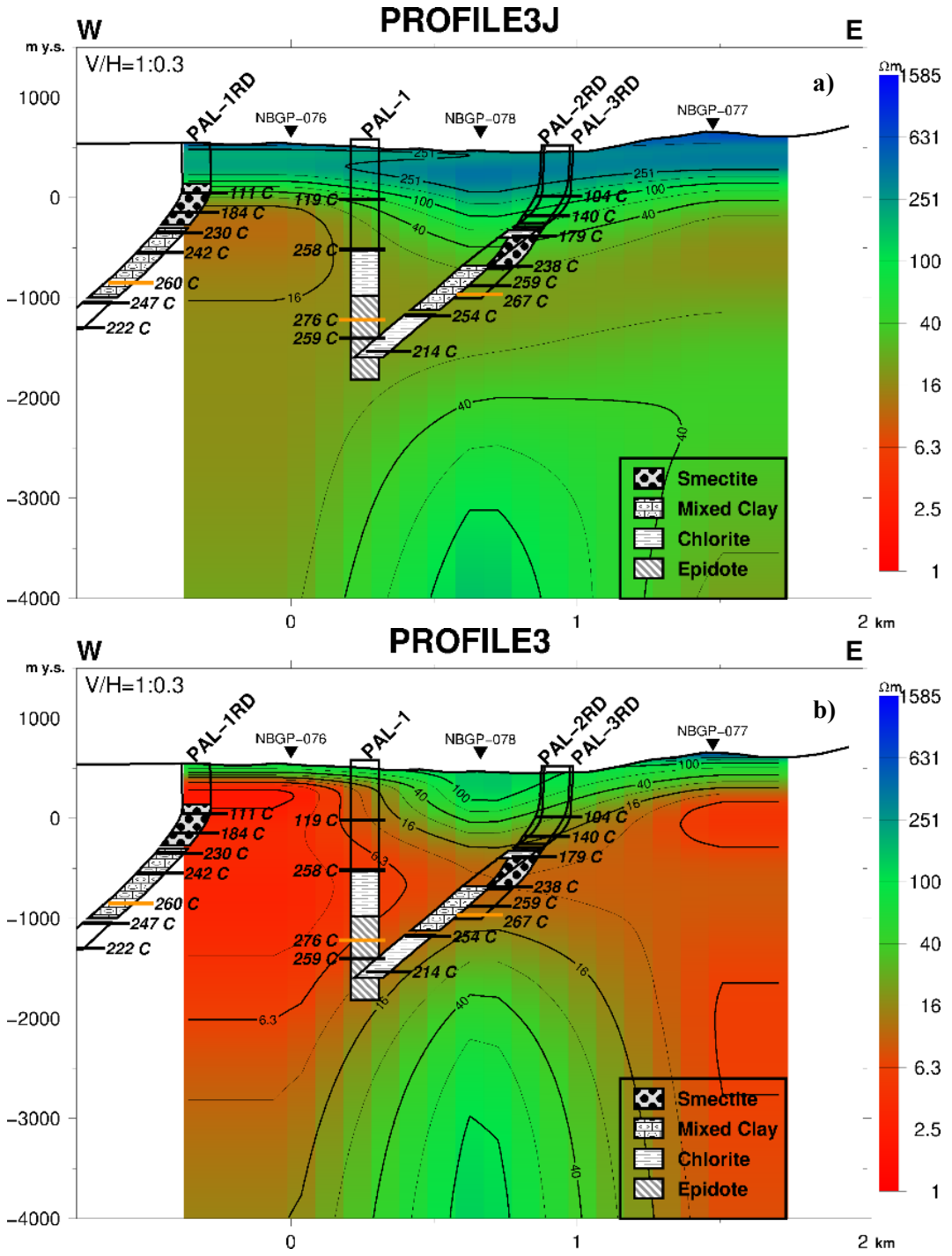

FIGURE 23: a) Jointly inverted b) MT inverted profile 3 running W-E extending up to a depth of 4000 m with 4 projected wells; better correlation of well alteration data observed in the jointly-inverted case than in the non-joint case (see Figure 19 for location)

We took a 2 km profile in the eastern part of the area where some wells are located. Profile 3, shown in Figure 19, considers 4 nearby wells which are mostly reinjection wells except for one, i.e. Well PAL-1, which is also farthest from the profile (around 500 m). Figure 23 shows two cases of inversion done in the same profile. The model generated from joint inversion is shown in Figure 23a (referred to from here on as joint case) while the model from MT inversion is shown in Figure 23b (referred to from here on as non-joint case). There is temperature inversion in the area with relic alteration observed mostly in the deeper regions of the wells. The maximum temperature reaches to around 270°C at 1500 m depth. The two sections show a big dissimilarity in their resistivity values at different depths. Joint case shows

severe shifting (~0.2-0.3) on both ends of the profile. The non-joint case indicates significantly thick and low-resistivity values of less than 10 Ωm extending up to 4000 m depth while the joint case indicates a thinner low-resistivity layer reaching up to 20 Ωm. Alteration minerals in the wells were also correlated with both of the profiles. In PAL-1RD, a relatively good overlap of smectite is seen with the decreasing resistivity region for both cases. However, the range of resistivity is much lower in the non-joint case but extends further on top of the identified smectite layer. The rest of the well's alteration information cannot possibly be correlated due to lack of sounding data. In PAL-1, better correlation of chlorite and epidote at depth of 1000-2500 m with resistivity is observed with the joint case than with the non-joint case where it intersects the profile at a low-resistivity value of around 10 Ωm. The first 350 m of the well is composed of unaltered andesitic lava flows (Reyes, 1982) and is distinctly identified by the joint case as a high-resistivity top layer of several hundreds of ohm-metres in value. In PAL-2RD and PAL-3RD (alteration data from Barnett, 1985), there is better overlap of smectite on the resistivity structure with the non-joint case but the relic chlorite found at shallower depth fits suitably with the joint case. Mixed clays and chlorite found at 1200-2100 m depth coincide more appropriately with the 20-40 Ωm range in the joint case than <16 Ωm range in the non-joint case. In this case, it can be considered that the resistivity profile of the jointly inverted data matches the alteration data of the nearby wells. But, it is good to realize that TEM data collected along this profile are shallow and there is no good overlap in the inversion. But the best model generated gave a considerably low misfit.

7. CONCLUSIONS AND RECOMMENDATIONS

1D joint inversion of the TEM data and the determinant of MT data in both Krýsuvík high-temperature area and Bacman geothermal area were done. It was observed that apparent resistivity offset is vulnerable in the areas. This has a lot of effect in the later inversion and interpretation if not considered beforehand. Highly probable areas of resistivity offset in a high-temperature geothermal environment are sites of altered grounds, thermal manifestations, huge topographic contrast, intrusive bodies and fractures occurring at the surface or the near-surface. A considerable amount of overlap of the late time TEM and the high-frequency MT data points must be established in order to obtain reliable inversion results, especially with the static shift parameter determination. This is done to increase confidence in the input data by reducing/removing unwanted 3D structure effects on the TEM data at late time and the downward bias at the high frequency range of MT data. The final model from a joint inversion using TEMTD satisfies a minimum misfit of the response curve with both TEM data and the shifted apparent resistivity MT data and its phase. A static shift parameter was also considered by the inversion in its model generation. The convergence to a best and acceptable fit is usually dependent on the initial model and the parameters imposed in the inversion.

The TEM method is unaffected by static shift but may produce data deviating from the true value even after multiple stacking. This may be caused by coupling, especially from nearby man-made electrical structures or some disturbances from communication equipment or facilities (Christiansen et al., 2006). Random noises from natural electromagnetic activity like spherics can also influence TEM data collection although they have very little effect (Christiansen et al., 2006). Some TEM data in Bacman were viewed as highly suspicious of being affected by some of these influences.

Shallow TEM soundings have been proven to be as important as deeper MT soundings in geothermal exploration. It is, thus, a good practice to have deeper TEM soundings by implementing larger transmitter loop areas, if possible, and applying a lower repetition rate to the transmitter current (30 Hz or less, in a 60 Hz power line environment). The depth of TEM sounding also relies on the subsurface resistivity such that TEM probes deeper in a resistive earth than a conductive earth, the same as with MT soundings. In order to have an increased signal to noise ratio of a TEM sounding, especially at late times, it is beneficial to increase the moment of the source loop by increasing its area, loop turns and/or the current amplitude but this, in general, is limited by the power rating of the transmitter instrument. It

is also a good strategy to implement different receiver loop areas to accommodate good quality data at various gate locations.

In implementing 1D joint inversion of MT and TEM data, it is always good to keep in mind that the unavoidable presence of 3D effects in the soundings are considered as noise just like electromagnetic disturbances. Thus, models generated from this inversion serve as a coarse model of the earth's resistivity structure.

ACKNOWLEDGEMENTS

I would like to express my warmest thanks to UNU-GTP staff for making the training as enjoyable and worthwhile as it can get. Your hospitality, patience and professionalism made this training a success. Best regards is also expressed to Dr. Ingvar Fridleifsson (retired UNU-GTP founding Director) for sharing a huge part of his life in honing geothermal talents all over the world and to Mr. Lúdvik S. Georgsson (current UNU-GTP Director) for keeping up the same vision that made this institution. I'm really humbled by your dedication. I am also deeply thankful to have as my supervisors Mr. Gylfi Páll Hersir and Mr. Andemariam Teklesenbet for their tireless encouragement and support during our project period. I salute your bountiful patience towards us, geophysical exploration trainees. I also greatly appreciate the efforts of the rest of my mentors in ÍSOR, Orkustofnun, especially Mr. Knútur Árnason, Mr. Arnar Már Vilhjálmsson, Mr. Gudni Karl Rosenkjaer and, again, Mr. Gylfi Páll Hersir for a handful of knowledge I gained regarding MT, TEM and all that comes along with it. You made me realize that geophysicists must think more than usual.

I also thank my employer, Energy Development Corporation Philippines, and my supervisor, Mr. Domingo Layugan, for giving me this opportunity to undergo geothermal training in Iceland. I am likewise grateful for the Filipino community in Iceland, especially the Torres family and relatives, who have helped me through the rest of my life here in this country. I will treasure our times together.

I thank my family for giving me unending support and inspiration to pursue my career as a geophysicist. You have always been and will be my sturdy foundation. Utmost gratitude will forever be expressed to God, our Grand Designer, for giving me life.

REFERENCES

Africa, J.R., 2013: Appendices to the report:*"1D inversion of MT and TEM data with application of soundings from Krýsuvík, SW-Iceland and a review of MT/TEM data from Bacman geothermal project, Central Philippines"*. UNU-GTP, Iceland, report 5 appendices, 50 pp.

Archie, G.E., 1942: The electrical resistivity log as an aid in determining some reservoir characteristics. *Tran. AIME, 146,* 54-67.

Árnason, K., 1989: *Central loop transient electromagnetic sounding over a horizontally layered earth*. Orkustofnun, Reykjavík, report OS-89032/JHD-06, 129 pp.

Árnason, K., 2006a: *TemX short manual*. ÍSOR – Iceland GeoSurvey, Reykjavík, internal report, 17 pp.

Árnason, K., 2006b: *TEMTD (Program for 1D inversion of central-loop TEM and MT data)*. ÍSOR – Iceland GeoSurvey, Reykjavík, short manual, 16 pp.

Árnason, K., Eysteinsson, H., and Hersir, G.P., 2010: Joint 1D inversion of TEM and MT data and 3D inversion of MT data in the Hengill area, SW Iceland. *Geothermics*, *39*, 13-34.

Arnórsson, S., Björnsson, A., and Gíslason, G., 1975: *Systematic exploration of the Krýsuvík high-temperature area, Reykjanes Peninsula, Iceland.* Orkustofnun, Reykjavik, report OS-JHD-7528, 20 pp.

Barnett, P.R., 1985: Memorandum: *Petrology report Bacman well PAL-3RD.* KRTA, report, 23 pp.

Bostick, F.X.Jr., 1986: Electromagnetic array profiling (EMAP). *56th Annual SEG Meeting, Houston, Texas, Expanded abstract, EM 2.1,*60–61.

Braganza, J.S., 2011: *Resource assessment update of Bacon-Manito geothermal resource*. Energy Development Corporation, Philippines, report, 66 pp.

Cagniard, L., 1953: Basic theory of the magneto-telluric method of geophysical prospecting. *Geophysics, 18,* 605-635.

Castells, A.M., 2006: *A magnetotelluric investigation of geoelectrical dimensionality and study of the Central Betic crustal structure*. University of Barcelona, Department of Geodynamics and Geophysics, PhD thesis, 45 pp.

Christiansen A.V., Auken E., and Sørensen K., 2006: The transient electromagnetic method. In: Kirsch R. (ed.), *Groundwater geophysics: a tool for hydrogeology*. Springer, NY, 179-225.

Constable, S.C., Parker, R.L., and Constable, C.G., 1987: Occam´s inversion: A practical algorithm for generating smooth models from electromagnetic sounding data. *Geophysics, 52-3,* 289-300.

Dakhnov, V.N., 1962: Geophysical well logging. *Q. Colorado Sch. Mines, 57-2*, 445 pp.

DeGroot-Hedlin, G., 1991: Removal of static shift in two dimensions by regularized inversion. *Geophysics, 56*, 2102–2106.

Flóvenz, Ó.G., Hersir, G.P., Saemundsson, K., Ármannsson, H., and Fridriksson Th., 2012: Geothermal energy exploration techniques. In: Syigh, A. (ed.), *Comprehensive renewable energy, vol. 7.* Elsevier, Oxford, 51-95.

Flóvenz, Ó.G., Spangerberg, E., Kulenkampff, J., Árnason, K., Karlsdóttir, R., Huenges, E., 2005: The role of electrical interface conduction in geothermal exploration. *Proceeding of the World Geothermal Congress 2005, Antalya, Turkey,* 9 pp.

Gamble, T.D., Goubau W.M., and Clarke, J., 1979: Magnetotellurics with a remote magnetic reference. *Geophysics, 44*, 53-68.

Geonics Ltd., 1999: *Operating manual for PROTEM 67 D.* Geonics Ltd, Ontario, 58 pp.

Georgsson, L.S., 2012: Geophysical methods in geothermal exploration. *Paper presented at "Short Course VII on Exploration for Geothermal Resources", organized by UNU-GTP and KenGen, at Lake Bogoria and Lake Naivasha, Kenya,* 16 pp.

Hersir, G.P., and Árnason K., 2009: Resistivity of rocks. *Paper presented at "Short Course on Surface Exploration for Geothermal Resources", organized by UNU-GTP and LaGeo, Santa Tecla, El Salvador*, 8 pp.

Hersir, G.P., Árnason, K., and Vilhjálmsson, A.M., 2013: 3D inversion of magnetotelluric (MT) resistivity data from Krýsuvík high temperature geothermal area in SW Iceland. *Proceedings of the 38th Workshop on Geothermal Reservoir Engineering, Stanford University, Stanford, Ca*, 14 pp.

Hersir, G.P., Vilhjálmsson, A.M., Rosenkjaer, G.K., Eysteinsson, H., and Karlsdóttir, R., 2010: *"The Krýsuvík geothermal field. Resistivity soundings 2007 and 2008".* ÍSOR – Iceland GeoSurvey, report ÍSOR-2010/025 (in Icelandic), 263 pp.

Jones, A.G., 1988: Static shift of magnetotelluric data and its removal in a sedimentary basin environment. *Geophysics, 53-7*, 967-978.

Keller, G.V., and Frischknecht, F.C., 1966: *Electrical methods in geophysical prospecting.* Pergamon Press Ltd., Oxford, 527 pp.

Lagmay, A.M.F, Tengonciang, A.M.P., and Uy, H.S., 2005: Structural setting of the Bicol basin and kinematic analysis of fractures on Mayon Volcano, Philippines. *J. Volcanology & Geothermal Research, 144,* 1-14.

Lemma Didana, Y., 2010: *Multidimensional inversion of MT data from Krýsuvík high-temperature geothermal field, SW-Iceland, and study of how 1D and 2D inversion can reproduce a given 2D/3D resistivity structure using synthetic MT data.* University of Iceland, MSc thesis, UNU-GTP, report 4, 94 pp.

Lund, J.W., Freeston, D.H., and Boyd, T.L., 2011: Direct utilization of geothermal energy 2010 worldwide review. *Geothermics*, *40*, 159-180.

Panem, C.C., and Alincastre, R.S., 1985: *Surface geology of the Bacon-Manito geothermal reservation.* Philippine National Oil Corporation – Energy Development Corporation, report.

Reyes A.G., 1982: *Petrological report: well Palayangbayan-1, Bacon-Manito Albay/Sorsogon.* Philippine National Oil Company- Energy Development Corporation, Philippines, memorandum, 6 pp.

SEG, 1991: *MT/EMAP data interchange standard*. Society of Exploration Geophysicists, 112 pp.

Simpson, F., and Bahr, K., 2005: *Practical magnetotellurics*. Cambridge University Press, Cambridge, UK, 254 pp.

Srivastava S.V., 1965: Methods of interpretation of magnetotelluric data when the source field is considered. *J. Geophys. Res., 70*, 945-954.

Sternberg, B.K., Buller, P.L., Kisabeth, J.L., and Mehreteab, E., 1982: Electrical methods for hydrocarbon exploration: II. Magnetotelluric (MT) method. *Proceedings Southern Methodist University Symposium III, Unconventional Methods in Exploration for Petroleum and Natural Gas.* SMU Press, 1984, 202-230.

Sternberg, B.K., Washburne, J.C., and Anderson, R.G., 1985: Investigation of MT static shift correction methods. *55th SEG meeting, Washington DC, Expanded Abstracts,* 264-267.

Todd, D.K., and Mays, L.W., 2005: *Groundwater hydrology* (3rd ed.). John Wiley & Sons, Inc., NY, 636 pp.

Vozoff, K., 1990: Magnetotellurics: principles and practice. *Proceedings of the Indian Academy of Sciences-Earth and Planetary Sciences, 99,* 441-471.